JCI The Journal of Clinical Investigation

S1PR1 inhibition induces pro-apoptotic signaling in T cells and limits humoral responses within lymph nodes

Dhaval Dixit, … , Jordan E. Axelrad, Susan R. Schwab

J Clin Invest. 2024. https://doi.org/10.1172/JCI174984.

Research In-Press Preview **Immunology**

Graphical abstract

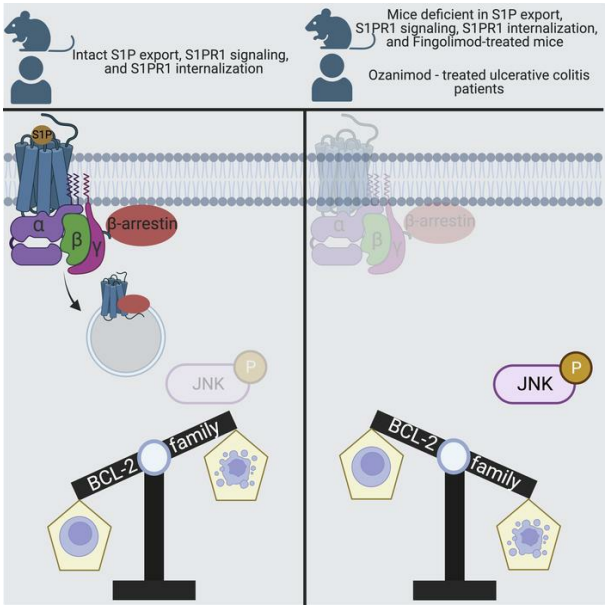

Find the latest version:

https://jci.me/174984/pdf

S1PR1 inhibition induces pro-apoptotic signaling in T cells and limits humoral responses within lymph nodes

Dhaval Dixit[1], Victoria M. Hallisey[1], Ethan Y.S. Zhu[1], Martyna Okuniewska[1], Ken Cadwell[2], Jerry E. Chipuk[3], Jordan E. Axelrad[4], Susan R. Schwab[1,*]

[1]Departments of Cell Biology and Pathology, New York University Grossman School of Medicine, New York, NY 10016, USA

[2]Department of Medicine and Institute for Immunology, University of Pennsylvania Perelman School of Medicine, Philadelphia, PA 19104, USA

[3]Department of Oncological Sciences, Department of Dermatology, and Tisch Cancer Institute, Icahn School of Medicine at Mount Sinai, New York, NY 10029, USA

[4]Division of Gastroenterology, Department of Medicine, New York University Grossman School of Medicine, New York, NY 10016, USA

*Correspondence: Susan R. Schwab; NYU Grossman School of Medicine, 430 E. 29th St. Floor 4, NY NY 10016; +1 415-385-1344; Susan.Schwab@nyulangone.org

Conflicts of interest: S.R.S. is an inventor on provisional patent 63/413,443 (Inhibitors of SPNS2 and uses thereof). K.C. has received research support from Pfizer, Takeda, Pacific Biosciences, Genentech, and Abbvie. K.C. has consulted for or received an honorarium from Puretech Health, Genentech, Abbvie, GentiBio, and Synedgen. K.C. is an inventor on U.S. patent 10,722,600 and provisional patents 62/935,035 and 63/157,225. J.E.A. has received research support from BioFire Diagnostics, and consultancy fees, honoraria, or advisory board fees from BioFire Diagnostics, Janssen, Pfizer, BMS, and Abbvie.

Abstract:

Effective immunity requires a large, diverse naïve T cell repertoire circulating among lymphoid organs in search of antigen. Sphingosine 1-phosphate (S1P) and its receptor S1PR1 contribute by both directing T cell migration and supporting T cell survival. Here, we addressed how S1P enables T cell survival, and the implications for patients treated with S1PR1 antagonists. We found that S1PR1 limited apoptosis by maintaining the appropriate balance of BCL2 family members via restraint of JNK activity. Interestingly, the same residues of S1PR1 that enable receptor internalization were required to prevent this pro-apoptotic cascade. Findings in mice were recapitulated in ulcerative colitis patients treated with the S1PR1 antagonist ozanimod, and the loss of naïve T cells limited B cell responses. Our findings highlighted an effect of S1PR1 antagonists on the ability to mount immune responses within lymph nodes, beyond their effect on lymph node egress, and suggested both limitations and additional uses of this important class of drugs.

Introduction

Regulated cell death is an integral process in mammalian development and homeostasis. T cells are often described as "primed" for apoptosis; developing T cells with non-functional or self-reactive T cell receptors must be eliminated(1, 2), and the bulk of effector T cells in an immune response must die to prevent excessive inflammation(3). However, naïve T cells must be long-lived to maintain a diverse repertoire to defend against diverse pathogens, and memory T cells must be long-lived to confer lasting protection(4, 5). A T cell makes critical decisions about whether to live or die at each stage of its life, and the factors that the cell weighs remain incompletely understood.

The signaling lipid sphingosine 1-phosphate (S1P) has been intensively studied in the context of T cell migration(6). The high concentration of S1P in blood and lymph guides T cells out of the low-S1P environment of lymphoid organs, and T cells follow this gradient primarily using S1P receptor 1 (S1PR1). Without circulatory S1P or without S1PR1 on T cells, T cells fail to exit the thymus into blood, and fail to exit lymph nodes (LN) into lymph. We have found that S1P, acting via S1PR1, also plays an essential role in naïve T cell survival, which interestingly is independent of its role in cell migration(7).

Four drugs that target S1PR1 have been FDA-approved to treat multiple sclerosis, and two have been approved to treat ulcerative colitis. These drugs work in part by blocking pathogenic T cells from exiting LN, thus preventing them from accessing the brain or colon(8, 9). However, some effects of these drugs are unexplained. Patients treated with drugs targeting S1PR1 respond poorly to SARS-CoV-2 vaccines(10-12), although B cell responses should be initiated within LN. Moreover, antibody titers have been reported to correlate negatively with time on drug, while the drugs' effects on cell migration occur within hours of the first dose and rapidly reach a new equilibrium(10-12). Finally, the few studies measuring blood lymphocyte counts in patients who have stopped treatment suggest that some patients do not fully recover cell numbers(13, 14).

We know little about how S1P supports T cell survival, or about how the effects of genetic blockade of S1P signaling in mice translate to the many patients treated with drugs targeting S1PR1. Here we addressed these questions. We found that S1PR1 activation restricted JNK phosphorylation, thereby maintaining the appropriate balance of BCL2 family members within the T cell, and in turn limiting apoptosis. Interestingly, the same residues of the S1PR1 C-terminus that enable receptor internalization were required to prevent the apoptotic cascade. Findings using genetic models were recapitulated in mice treated with the drug fingolimod (FTY720), which targets S1PR1, and in ulcerative colitis patients

treated with the drug ozanimod, also an S1PR1 modulator. Using a mouse model, we found that poor antibody responses after prolonged treatment with S1PR1 antagonists may in part reflect loss of the naïve T cell repertoire, pointing to an important role of S1P signaling in regulating T cell responses within the LN as well as in non-lymphoid tissues. Our findings simultaneously suggest reasons for caution in use of S1PR1 antagonists and additional uses for these drugs.

Results

The S1P transporter SPNS2 and S1PR1 prevent naïve T cell death

We began by further testing the role of S1P in promoting naïve T cell survival. We had previously shown that in mice lacking the S1P transporter SPNS2 in *Lyve1*-expressing cells, which include lymphatic endothelial cells (*Spns2*$^{f/f}$ *Lyve1*-Cre, *Spns2*Δ^{Lyve1}), lymph S1P was lost (Figure S1A)(7). As expected, naïve T cells were retained in LN because there was no lymph S1P to guide them out, and naïve T cells were no longer exposed to circulatory S1P(7). Surprisingly, they died at an increased rate compared to T cells in LN of littermate controls(7). To assess potential developmental defects contributing to T cell death, we deleted *Spns2* in adults. We bred *Spns2*$^{f/f}$*UBC*-CreERT2 mice, with widespread expression of tamoxifen-inducible Cre(15), and treated adults with tamoxifen 3 weeks before analysis (tamoxifen-treated *Spns2*$^{f/f}$*UBC*-CreERT2 mice, *Spns2*Δ^{UBC}). We measured cell death by flow cytometry, assessing propidium iodide uptake as well as staining with a probe for active caspases and with Annexin V (Figure 1A). We found an increased percent of dying cells among naïve T cells in *Spns2*Δ^{UBC} LN compared to tamoxifen-treated littermate controls, as well as a loss of naïve T cells (Figures 1B and S1B-S1D). Consistent with the importance of S1P secretion by SPNS2, we found an increased percent of dying cells among naïve T cells in LN of mice with *Lyve1*-Cre-mediated deletion of the two sphingosine kinases that synthesize S1P (*Sphk1*$^{f/f}$*Sphk2*$^{-/-}$*Lyve1*-Cre, *Sphk*Δ^{Lyve1})(16) (Figure S1E). Finally, we confirmed previous findings that S1PR1 was required in a cell-intrinsic manner to limit naïve T cell death, using mixed bone marrow chimeras and transfer experiments ((7) and below). These data suggest a model in which S1P secreted via SPNS2 and sensed by T cells via S1PR1 promotes naïve T survival.

S1P signaling promotes naïve T cell survival independent of exit from LN or uptake of S1P

S1P could promote naïve T cell survival by at least three possible mechanisms: enabling T cell trafficking among or within lymphoid organs, acting as a metabolite or protein co-factor after uptake into the T cell, or activating a signaling pathway downstream of S1PR1 within the T cell.

Our previous work had indicated that S1PR1 did not promote survival by enabling exit from LN or access to IL7 or peptide-MHC within LN ((7) and below). We next considered the hypothesis that S1P uptake was important for T cell survival. S1PR1 is a G-protein-coupled receptor (GPCR), and, like many GPCR, S1PR1 is internalized after binding its ligand(17, 18). Intracellular S1P has been implicated in many processes important for cell survival, from acting as a metabolic intermediate to promoting mitochondrial homeostasis to regulating glycolysis(19-22). To test the role of S1P uptake by S1PR1 in T cell survival, we took advantage of a chemical agonist of S1PR1, SEW-2871, which is structurally distinct from S1P(23). We treated *Spns2*Δ^{Lyve1} mice and littermate controls with SEW-2871 or vehicle daily for 10d (Figure 1C). Naïve T cells in both *Spns2*Δ^{Lyve1} mice and controls treated with SEW-2871 expressed lower levels of surface S1PR1 than naïve T cells in vehicle-treated mice (Figure 1D), consistent with previous findings that SEW-2871 bound the receptor and induced its internalization. As expected, in *Spns2*Δ^{Lyve1} mice, the increased S1PR1 signal in LN did not restore egress. As expected, in control mice, increased agonism of S1PR1 in LN disrupted the ligand gradient that would normally guide exit from LN (normally low S1PR1 agonism in LN, now elevated due to the presence of SEW-2871; normally high S1PR1 agonism in lymph, still high with the continued presence of S1P) (Figure S1F). We found that SEW-2871-treated *Spns2*Δ^{Lyve1} mice had a reduced frequency of dying naïve T cells compared to vehicle-treated *Spns2*Δ^{Lyve} mice (Figures 1E and S1G-S1H). This result suggested that signaling through S1PR1, rather than S1P uptake (or LN exit), was important for naïve T cell survival. Importantly, SEW-2871 treatment of *S1pr1*Δ^{UBC} mice did not rescue naïve T cell apoptosis (Figures 1F-1G), indicating that SEW-2871 worked through S1PR1 to promote survival.

Naïve T cell apoptosis is not associated with changes in canonical signaling pathways downstream of S1PR1

We then considered the possibility that S1PR1 activates a pro-survival signaling pathway within naïve T cells. S1PR1 couples to $G\alpha_i$ and its associated $G\beta\gamma$ subunits(24). Experiments using cultured cells have demonstrated that S1PR1, like many GPCR, can activate AKT and ERK, kinases that promote survival in many contexts(25, 26). Furthermore, $G\alpha_i$ inhibition of adenylate cyclase has been demonstrated in many cell types to prevent cAMP accumulation and hence limit protein kinase A (PKA) activation. Yet little is known about S1PR1-dependent signaling pathways in naïve T cells in vivo. In LN, T cells receive inputs from many other sources including cytokine receptors, chemokine receptors, the T cell receptor, and metabolic sensors, and these also regulate AKT, ERK, and/or PKA signaling. We therefore asked whether S1PR1's contribution was limiting in the context of the many other inputs into these pathways in a naïve T cell in vivo.

To study S1PR1's contribution to AKT and/or ERK activation, we measured AKT and ERK phosphorylation in naïve T cells from *Spns2*Δ^{Lyve1} and *S1pr1*Δ^{UBC} mice and littermate controls. We predicted that expression of pAKT or pERK would be decreased in naïve T cells from *Spns2*Δ^{Lyve1} and *S1pr1*Δ^{UBC} mice if S1P signaling were a key input to the pathway. We detected no difference in pAKT or pERK in naïve T cells between *Spns2*Δ^{Lyve1} mice and littermate controls. This could have simply reflected a limitation of the assay, but naïve T cells from *S1pr1*Δ^{UBC} mice had reproducibly ***increased*** levels of pAKT and pERK compared to littermate controls (Figures 2A-2C). Since activity of these pathways was not decreased, we concluded that they were unlikely to account for S1P-dependent naïve T cell survival. We were surprised by the divergence between *Spns2*Δ and *S1pr1*Δ T cells in pAKT and pERK levels; we ultimately found that differential expression of the C-type lectin CD69 explained the difference (Supplemental Figure 2).

We also tested whether $G\alpha_i$ inhibition of cAMP-PKA was important for S1P-dependent naïve T cell survival. Activated PKA can phosphorylate the transcription factor CREB(27). We found that naïve T cells from both *Spns2*Δ and *S1pr1*Δ mice had slightly increased phosphorylated CREB, suggesting that S1PR1's input was limiting for inhibition of the cAMP-PKA-CREB pathway (Figures 2D-2E). To test whether this pathway was important in naïve T cell survival, we treated *S1pr1*Δ mice daily with a PKA inhibitor, H89 (28) (Figure 2F). Although the inhibitor reduced CREB phosphorylation, it did not affect the frequency of dying naïve T cells, suggesting that a PKA-dependent pathway did not regulate S1P-dependent naïve T cell survival (Figures 2G-2H).

S1P signaling promotes survival by regulating the balance of BCL2 family proteins

We next investigated whether loss of S1PR1 signaling resulted in changes in proximal regulators of cell death; we hoped to use this information to work back to the receptor.

Analysis of RNA and protein indicated that the balance of BCL2 family members was altered upon loss of S1P signaling. Using RNA-Seq, we compared transcripts of *S1pr1*Δ^{UBC} and littermate control naïve T cells, isolated from mixed bone marrow chimeras in which *S1pr1*$^{f/f}$*UBC*-CreERT2 and control bone marrow was used to reconstitute WT hosts. We also compared transcripts of naïve T cells from chimeras in which WT bone marrow was used to reconstitute either *Spns2*Δ^{Lyve1} or littermate control hosts. Two genes within the BCL2 family were altered upon loss of S1P signaling: the anti-apoptotic gene *Bcl2* (BCL2) was down-regulated (more consistently in SPNS2-deficient than S1PR1-deficient T cells), and the pro-apoptotic gene *Bbc3* (PUMA) was up-regulated (Figure S3A). Using flow cytometry to measure intracellular protein, we found that naïve T cells from *Spns2*Δ and *S1pr1*Δ mice had an approximately 20-25% reduction in BCL2 staining compared to littermate controls (Figures 3A-3B and S3D). Furthermore, we detected an approximately 20-25% increase in PUMA staining (Figures 3C-3D and S3E). Ultimately, apoptosis is executed by effectors, either BAX or BAK. Naive T cells from *Spns2*Δ and *S1pr1*Δ mice had an approximately 30% increase in BAX staining compared to controls (Figures 3E-3F and S3F). Because T cells are thought to be "primed" for apoptosis, this imbalance of BCL2 family members might trigger cell death via the mitochondrial pathway of apoptosis.

To assess whether an imbalance of BCL2 family members resulted in death upon loss of S1P signaling, we tested three predictions. First, we predicted that if *S1pr1*Δ T cells had a physiologically relevant imbalance of BCL2 family members, providing an additional stress that activated the mitochondrial pathway of apoptosis would lead to increased death of *S1pr1*Δ T cells compared to controls. We co-transferred *S1pr1*Δ and littermate control naïve T cells at a 1:1 ratio into WT recipients. One day after transfer, we treated the recipients with the BCL2-specific inhibitor ABT-199 (29), and one day after ABT-199 treatment, we enumerated transferred cells in LN (Figure 4A). We found that ABT-199 treatment led to a marked reduction in the ratio of *S1pr1*Δ to control T cells (Figure 4B). Similar in vivo experiments using dexamethasone or irradiation also led to a reduction in the ratio of *S1pr1*Δ to control T cells, suggesting that *S1pr1*Δ T cells were more susceptible than controls to pro-apoptotic stresses (Figures S3G-S3H). ABT-199 treatment ex vivo also led to increased cell death among *S1pr1*Δ cells than controls (Figures 4C-4D). By contrast, ex vivo treatment with Fas ligand led to similar cell

death among *S1pr1*Δ T cells and controls (Figures 4C and 4E), suggesting that *S1pr1*Δ T cells were not more susceptible to death via the extrinsic pathway of apoptosis.

Second, we predicted that if loss of S1P signaling led to an imbalance of BCL2 family members, then increasing T cell exposure to S1P in *Spns2*Δ mice should restore the balance. To test this, we took advantage of the finding that the enzyme S1P lyase maintains low levels of S1P in LN(18). We treated *Spns2*Δ^{UBC} and control mice with the S1P lyase inhibitor 4'deoxyhydropyridoxine (DOP) for 3 weeks (Figure S4A). As expected from previous studies(7), DOP treatment of *Spns2*Δ or control mice increased T cell exposure to S1P within LN, indicated by internalization of S1PR1 (Figure S4B). As expected, in *Spns2*Δ^{UBC} mice, increased LN S1P did not restore exit from LN; in control mice, increased LN S1P disrupted the gradient that would normally guide cells out of LN and limited exit (Figure S4C). As expected, DOP-treated *Spns2*Δ^{UBC} mice had a reduced frequency of dying naïve T cells compared to vehicle-treated *Spns2*Δ^{UBC} mice (Figures S4D-S4F). We assessed how DOP affected the levels of BCL2 family members in naïve T cells. We found that DOP treatment restored BCL2, PUMA, and BAX levels in naïve T cells from *Spns2*Δ mice to similar levels as controls, consistent with the hypothesis that S1P signaling maintains the balance of BCL2 family members in naïve T cells (Figures 4F-4G).

Last, we predicted that the imbalance of BCL2 family members would be the upstream cause of apoptosis in mice lacking S1P signaling. To test this, we took advantage of *Bax*$^{-/-}$ T cells(30), which lack one of the two pore-forming proteins that execute the mitochondrial pathway of apoptosis. We co-transferred T cells from *Bax*$^{-/-}$ mice and WT littermates into *Spns2*Δ^{Lyve1} mice and littermate controls. 3 weeks later, we enumerated the transferred cells (Figure 4H). Transferred WT and *Bax*$^{-/-}$ T cells were found in similar numbers in WT LN, while WT T cells decreased about 30% compared to *Bax*$^{-/-}$ T cells in *Spns2*Δ^{Lyve1} LN (Figure 4I). Although *Bax*$^{-/-}$ T cells survived better in Spns2Δ^{Lyve1} mice than control mice, *Bax*$^{-/-}$ T cells transferred into *Spns2*Δ mice still had lower levels of BCL2 and higher levels of PUMA than *Bax*$^{-/-}$ T cells transferred into controls (Figures 4J and S4G). This result suggested that imbalance of these proteins preceded death.

These data suggest that lack of S1P signaling leads to an imbalance in BCL2 family proteins, which promotes naïve T cell apoptosis. Of course, additional changes in BCL2 family members beyond those that we measured may also contribute to this imbalance.

S1P signaling regulates the balance of BCL2 family members by restraining JNK activation

The expression and function of BCL2 family members are regulated by multiple pathways, including JNK signaling(31). Prolonged JNK activation can promote apoptosis(32). We therefore tested whether JNK was activated in cells lacking S1P signaling. We measured phosphorylation of JNK and one of its downstream targets, the transcription factor cJun, by flow cytometry. Naïve T cells from LN of both *Spns2*Δ and *S1pr1*Δ mice had reproducibly increased expression of phosphorylated JNK1/2 (pJNK) and phosphorylated cJun (pcJun) compared to controls (Figures 5A-5B, S5A-S5B). JNK can be activated by the kinases MKK4 and MKK7 (32), and we detected increased phosphorylated MKK7 (pMKK7) in naïve T cells from *Spns2*Δ and *S1pr1*Δ mice (Figures 5C and S5C).

To assess whether JNK activation resulted in the imbalance of BCL2 family members and increased apoptosis in the absence of S1P signaling, we tested three predictions. First, we predicted that decreasing JNK activity would restore levels of BCL2 family members and T cell survival. We treated *S1pr1*Δ mice with one of two structurally distinct JNK inhibitors, SP600125 (33) or JNK-IN-8 (34), or vehicle for 10 days (Figure 5D). JNK inhibition effectively reduced levels of pcJun (Figure 5E). We found that JNK inhibition decreased the frequency of dying naïve T cells in LN (Figure 5F), and this was accompanied by increased BCL2 and decreased PUMA and BAX (Figure 5G).

Second, we predicted that if loss of S1P signaling led to JNK activation, then increasing T cell exposure to S1P in *Spns2*Δ mice should reduce pJNK. We treated *Spns2*Δ^{UBC} and littermate control mice with DOP for 3 weeks to increase LN S1P. We found that DOP treatment restored pJNK in naïve T cells from *Spns2*Δ mice to levels similar to controls (Figure 5H).

Last, we predicted that JNK activation would be the upstream cause of apoptosis in mice lacking S1P signaling. To test this, we again took advantage of *Bax*$^{-/-}$ T cells, which partly recovered in numbers in *Spns2*Δ hosts. We transferred *Bax*$^{-/-}$ lymphocytes into *Spns2*Δ mice or controls and measured levels of pJNK and pMKK7 3 weeks later. *Bax*$^{-/-}$ T cells in *Spns2*Δ mice had elevated pJNK and pMKK7 compared to *Bax*$^{-/-}$ T cells in controls (Figures 5I and S5D), suggesting that JNK activation preceded death.

These results suggest that loss of S1P signaling results in JNK activation, which in turn alters the balance of BCL2 family members and leads to apoptosis.

JNK activation is not explained by loss of mitochondria

JNK can be activated by many types of cellular stress(32). We had previously observed that *S1pr1*Δ naïve T cells had decreased mitochondrial content(7), and we asked whether altered mitochondria could be the key stressor. We analyzed mitochondria in naïve T cells by electron microscopy (Figure S5E). We found that mitochondria in *S1pr1*Δ naïve T cells had decreased cross-sectional area compared to mitochondria in controls, and that *S1pr1*Δ naïve T cells had a slightly increased number of mitochondria per cell compared to controls (Figures S5F-I). However, we did not detect differences in cross-sectional area of mitochondria or number of mitochondria in naïve T cells from *Spns2*Δ mice compared to controls (Figures S5F-I). We did not observe striking differences in mitochondrial cristae organization between either *S1pr1*Δ mice or *Spns2*Δ mice and controls. While the mitochondrial changes are very interesting, they are unlikely to explain JNK activation because they are divergent between *S1pr1*Δ and *Spns2*Δ T cells.

JNK activation correlates with loss of S1PR1 internalization

To address how S1P/S1PR1 restrain JNK, we turned to our RNA-Seq datasets. Interestingly, we found dysregulation of genes related to endocytosis and the actin cytoskeleton in both T cells lacking S1PR1 and T cells from SPNS2-deficient mice (Figure S3B-C). One striking quality of S1PR1 is that it is extremely susceptible to ligand-induced endocytosis by concentrations of S1P encountered in vivo. During a T cell's continual trafficking among lymphoid organs, S1PR1 is cyclically lost from the cell surface in the high-S1P environment of blood and lymph, and returned to the cell surface in the low-S1P environment of lymphoid organs(35). We therefore considered the possibility that the constant endocytosis of the receptor itself was important for cell physiology, perhaps by affecting the actin cytoskeleton. Our data so far were consistent with a requirement for S1PR1 internalization in T cell survival. In *Spns2*Δ mice, where naïve T cells die, T cells in the LN maintain very high levels of surface S1PR1 due to lack of S1P exposure. In *Spns2*Δ mice treated with DOP or SEW-2871, naïve T cell survival is restored, and surface S1PR1 levels are reduced by ligand-induced internalization.

To test whether internalization of S1PR1 was important for naïve T cell survival, we took advantage of the knowledge that the kinase GRK2 induces S1PR1 internalization by phosphorylating the receptor's C-terminal tail and enabling β-arrestin to bind the receptor(36, 37). In *Grk2*$^{f/-}$CD4-Cre mice, naïve T cells maintain aberrantly high levels of

S1PR1 in blood and are present at reduced numbers in blood and secondary lymphoid organs(37). We generated bone marrow chimeras by reconstituting WT mice with congenically marked *Grk2*$^{f/-}$CD4-Cre (*Grk2*Δ) or *Grk2*$^{f/+}$CD4-Cre (Ctrl) bone marrow (Figure 6A). Eight weeks after reconstitution, we confirmed increased S1PR1 levels on naïve CD4+ T cells in blood (Figures 6B-6C). We found that LN of *Grk2*Δ mice had an increased frequency of dying naïve T cells, accompanied by increased JNK activation and an imbalance of BCL2 family members, with the exception of similar BCL2 expression between *Grk2*Δ and control naïve CD4 T cells (Figures 6D-6F). These results are largely consistent with the possibility that deficient S1PR1 internalization impairs naïve T cell survival, but interpretation is complicated by pleotropic functions of GRK2.

To study S1PR1 internalization more specifically, we manipulated the C-terminal tail of S1PR1, which has a series of serine and threonine residues that are phosphorylated by GRK2. Replacement of 5 serines in the C-terminal tail with alanine (S351A, S353A, S355A, S358A, S359A)(38) or of 2 serines and 1 threonine in the C-terminal tail with alanine (T371A, S374A, S375A)(37) had been shown to slow S1PR1 internalization, but in both cases surface S1PR1 remained undetectable on T cells in blood and no abnormalities in T cell numbers were reported. To more completely limit internalization, we mutated S1PR1 to substitute alanine for nine serines and one threonine in the C-terminal tail (ST10A) (Figure 7A). Naïve *S1pr1*Δ T cells were activated in culture; transduced with empty vector, S1PR1-WT, or S1PR1-ST10A; then rested for 3 days in IL7 and IL15 to generate CD8+ T cells with central-memory properties(39). Empty vector, S1PR1-WT, or S1PR1-ST10A-expressing *S1pr1*Δ T cells were transferred into recipients. 4-5 days later, the transferred T cells were analyzed (Figure 7B). S1PR1-ST10A-transduced *S1pr1*Δ T cells had higher levels of surface S1PR1 compared to S1PR1-WT-transduced *S1pr1*Δ T cells in blood and LN (Figures 7C-7E). While S1PR1-WT-transduced *S1pr1*Δ T cells had lower rates of apoptosis than empty vector-transduced *S1pr1*Δ T cells, S1PR1-ST10A-transduced T cells had similarly high rates of apoptosis to empty vector-transduced *S1pr1*Δ T cells (Figure 7F). Similarly, while S1PR1-WT-transduced *S1pr1*Δ T cells had lower levels of pJNK and higher levels of BCL2 than empty vector-transduced *S1pr1*Δ T cells, S1PR1-ST10A-transduced T cells had similar levels of pJNK and BCL2 to empty vector-transduced *S1pr1*Δ T cells (Figure 7G).

Taken together, these data suggest that phosphorylation of the C-terminal tail of S1PR1 regulates both receptor internalization and T cell survival, consistent with the possibility that endocytosis of S1PR1 restrains JNK activation, maintains the balance of BCL2 family members, and prevents apoptosis.

Chronic FTY720 treatment recapitulates apoptosis

S1PR1 modulators have had remarkable clinical efficacy treating multiple sclerosis and ulcerative colitis. FTY720, the most commonly used drug targeting S1PR1, acts as an agonist of S1PR1 in the short-term but as a functional antagonist of S1PR1 in the long-term in many contexts. After binding S1PR1 and inducing an acute signal through the receptor, FTY720 induces S1PR1 internalization and degradation, mimicking genetic loss of *S1pr1*(40). By contrast, S1P or SEW-2871 induce S1PR1 signaling and internalization, but S1PR1 is shuttled back to the cell surface where it can signal again(40). Recent studies measuring blood lymphocyte counts in patients who have stopped FTY720 treatment suggest that some patients do not fully recover cell numbers months after treatment cessation(13, 14). We hypothesized that FTY720 may not only block lymphocyte circulation but also induce naïve T cell death.

To test this, we treated WT mice with FTY720 or vehicle for 3 weeks (Figure 8A). We found an increased frequency of dying cells among naïve CD4 T cells in LN of FTY720-treated mice compared to controls, accompanied by increased pJNK and pMKK7, decreased BCL2, and increased PUMA and BAX (Figures 8B-8D). Although FTY720 has pleotropic effects, including blockade of thymic exit, these data are consistent with FTY720 acting as a functional antagonist of S1PR1 in the context of T cell death.

We next asked whether increased T cell death was also present in patients treated with S1PR1 modulators. We analyzed peripheral blood mononuclear cells (PBMC) from UC patients being treated with the S1PR1 modulator ozanimod(9) (Table 1, Figures 8E, S6A). We found an increased percentage of AnnexinV+ cells among naïve CD4+ T cells as well as naïve CD8+ and central memory CD4+ T cells in patients treated with ozanimod compared to healthy controls or UC patients on a different therapy (Figures 8F and S6B). We also detected increased activation of the JNK pathway and an imbalance of BCL-2 family members in T cells from ozanimod-treated patients compared to controls (Figures 8G-8H, S6C-S6D). These data suggest that loss of S1PR1 function in human T cells, as in murine T cells, not only disrupts their trafficking but also may lead to apoptosis.

Chronic FTY720 treatment reduces follicular T helper and germinal center B cell numbers

In response to the SARS-CoV-2 vaccine, patients on S1PR1 modulators have lower levels of anti-spike IgG antibody and lower seroconversion rates compared to patients treated with most other types of immune suppressants(41). Interestingly, the strength of the antibody response has been reported to correlate inversely with the duration of drug treatment before vaccination(11, 12), while effects of these drugs on lymphocyte trafficking should be rapid and sustained. We hypothesized that one mechanism for the reduced response is loss of the naïve T cell repertoire due to apoptosis(42).

To test this hypothesis, we studied the response of FTY720-treated mice to a T cell-dependent model antigen, sheep red blood cells (SRBC), injected subcutaneously. We enumerated follicular T helper cells (Tfh) and germinal center B cells (GCB) in the draining LN 8 days after immunization. We compared vehicle, 'short' FTY720 treatment (first dose 1 day prior to immunization), and 'long' FTY720 treatment (first dose 3 weeks prior to immunization) (Figure 9A). Interestingly, long FTY720 treatment led to a substantial reduction in the numbers of Tfh and GCB cells compared to other groups (Figures 9B-9D and S6E).

FTY720 targets multiple S1P receptors on numerous cell types(43, 44), any of which might contribute to the declining germinal center response over time. To test whether the reduced germinal center response was due to loss of the naïve T cell repertoire (which in FTY720-treated mice, as in patients, was due both to cell death and a loss of thymic exit), we asked whether we could restore the response by increasing the number of naive T cells (Figure 9E). We transferred polyclonal naïve T cells into FTY720-treated mice. As a control, we transferred the same number of ovalbumin-specific T cells into a second group of FTY720-treated mice. If the decreased germinal center response were due to a loss of the naïve T cell repertoire, ovalbumin-specific T cells should not restore it. The transferred cells were isolated from donors treated with FTY720 using the same protocol as recipients, to avoid unanticipated artefacts. Transfer of polyclonal T cells, but not ovalbumin-specific T cells, increased Tfh and GCB cell numbers (Figures 9F-9G). The rescue was incomplete, but we were unable to replenish the T cell pool fully. The number of GCB cells increased with the total number of T cells in the case of polyclonal T cell transfer (Figure S6F). As expected, transfer of ovalbumin-specific T cells did not result in a large increase in the total number of T cells, likely due to competition for a limited niche (Figure S6F)(45).

Discussion

Naïve T cell survival is crucial to maintain a diverse repertoire of T cells, which enables a robust immune response to a diverse range of pathogens. Here, we addressed how S1P and S1PR1 support naïve T cell survival, and whether this

pathway is disrupted in patients treated with S1PR1 antagonists. We found that S1P signaling through S1PR1 limits JNK activation, which in turn maintains the appropriate balance of BCL2 family members within the T cell, and thereby prevents apoptosis. Interestingly, T cells without S1P/S1PR1 signaling have differential expression of genes regulating endocytosis and the actin cytoskeleton compared to controls, and phosphorylation of the same residues of the S1PR1 C-terminus that enable ligand-induced internalization of S1PR1 also promotes S1PR1-dependent survival. FTY720, a functional antagonist of S1PR1 that is used extensively to treat patients with autoimmune disease, induces naïve T cell death via the same pathway as genetic deletion of SPNS2 and S1PR1. The loss of naïve T cells can limit generation of B cell responses.

Our work suggests that S1PR1 modulators currently used clinically to treat autoinflammatory diseases may induce naïve T cell apoptosis. Early studies aimed at understanding the lymphopenia induced by FTY720 found increased apoptosis of cells treated with the drug in vitro(46-48). Notably, one study found increased JNK activation(49), and another study found that BCL-2 overexpression prevented FTY720-induced apoptosis(47, 48). Together with many studies implicating S1P in cell survival, these experiments suggested that cell death could account for the lymphopenia and immunosuppression(19, 50, 51). In contrast, in vivo studies demonstrated that FTY720 induced lymphopenia by inhibiting egress of lymphocytes into lymph(44). Our experiments echo the early findings. FTY720's effects on cell death in vivo may have been discounted due to its more readily observable effects on cell trafficking.

One key future direction is to explore how these findings should alter clinical practice. Our work suggests that it will be important to consider effects of S1PR1 modulators on immune responses within the LN, as well as the more obvious effects on immune responses in non-lymphoid tissues. Reductions in naïve T cell numbers may limit the initiation of immune responses, and it will be important in future work to assess how chronic JNK signaling may affect T cell function. In some settings, this may be an unacceptable side-effect. In other settings, this may be beneficial, limiting the recruitment of new T cells into an immune response. Going forward, effects of targeting S1PR1 on the immune system must be assessed more holistically.

On the more basic side, an interesting question is how S1PR1 limits JNK activation. Our data suggest that S1PR1 internalization (or the amino acids that enable internalization) restrains JNK. We are considering three candidate mechanisms. First, S1PR1 might signal through a unique partner within endosomes or other intracellular compartment, which in turn might limit JNK phosphorylation. Intracellular functions of GPCR are increasingly appreciated(52); for example, after ligand-induced internalization, GPR35 traffics to the outer mitochondrial membrane, where it regulates

protein-protein interactions(53). Second, when S1PR1 cannot be internalized, the internalization machinery might be freed to associate with other receptors, which may result in JNK activation. For example, β-arrestin, a key regulator of GPCR internalization, has a MAP kinase docking site that can enable JNK activation in some settings(54, 55).

Third, loss of S1PR1 internalization might itself induce cell stress, which in turn could result indirectly or directly in JNK activation. Receptor internalization requires rearrangement of the actin cytoskeleton, and stabilization of actin filaments or alterations in actin binding proteins can induce JNK activation(56). Furthermore, S1PR1 has recently been shown to promote a unique form of bleb-based movement by utilizing Ezrin-Radixin-Moesin proteins, which form linkages between the plasma membrane and the actin network(26). Ezrin phosphorylation is associated with activation of MKK7 and JNK in B cells(57), suggesting the possibility that ezrin phosphorylation-dephosphorylation events may regulate actin dynamics and thereby affect cell survival. Interestingly, mice deficient in the actin regulators *Dock8* (58) or *Coro1a* (59, 60) have perturbed T cell homeostasis due to both migration defects and increased cell death. Lymphocytes must be able to deform in order to squeeze through endothelial barriers as well as to move within organs, and perhaps the same receptors that guide their migration keep the cytoskeleton flexible.

While role of S1PR1 in T cell egress from lymphoid organs is increasingly well understood, to the point at which five drugs targeting S1PR1 have been FDA-approved for treatment of inflammatory disease and more are in clinical trials, the role of S1PR1 in T cell survival has just begun to be explored. It will be essential to understand this pathway to better direct use of this powerful class of drugs.

Methods:

Study Design

For mice, sample sizes balanced statistical robustness and animal welfare, and negative results should not be over-interpreted. No animals were excluded from analysis unless they were clearly sick (hunched, low body weight). No specific method of randomization was used to allocate mice into groups, although sex-matched littermates were used when possible. For human samples, we analyzed blood from all consented patients who were treated with ozanimod at NYU Langone's Inflammatory Bowel Disease Center over 16 months, and consented controls who visited the clinic the same day. The order of sample collection and data acquisition was designed to avoid experimental bias: collection and processing of samples from control and knockout, as well as treated and untreated animals/people, were alternated. Investigators were not blinded, because there were no qualitative measurements. No outliers were excluded, and no experiment was excluded unless a positive or negative control failed.

Mice

C57BL/6J (WT; CD45.2), B6.SJL-*Ptprc*^{a}*Pepc*^{b}/BoyJ (CD45.1), *Spns2*$^{f/f}$(61), *S1pr1*$^{f/f}$(62), *Bax*$^{-/-}$(30), *Lyve1*-Cre(16), *UBC*-CreERT2(15), MHCII$^{-/-}$(63), *Cd69*$^{-/-}$(64), *Sphk1*$^{f/f}$(65), *Sphk2*$^{-/-}$(66), OT-I(67), and OT-II(68) mice have been previously described. All mice were bred in NYU School of Medicine animal facilities. Mice were on a C57BL/6 or, in some cases, a C57BL/6x129 background. Mice were always compared to littermate controls. Mice were 7–20 weeks old at the time of analysis. Male and female mice were used depending on availability, as sex did not seem to affect the results. Mice were housed in specific pathogen-free conditions. All cages were on a 12:12-h light:dark cycle (lights on, 07:00). Room temperature was maintained at 72 ± 2 °F (22.2 ± 1.1 °C), and room humidity was maintained at 30–70%.

Human blood samples

Peripheral blood was drawn from anonymous, adult IBD patients being treated with Zeposia (ozanimod), adult IBD patients being treated with a different therapy, or healthy control adults.

Treatments

Tamoxifen (Sigma-Aldrich) was dissolved in corn oil (Sigma-Aldrich) by shaking at 37°C for 3h, at 20mg/mL or 40mg/mL. 2mg tamoxifen was administered intraperitoneally on 5 consecutive days or 6mg tamoxifen was administered by gavage on 2 consecutive days. Unless otherwise indicated, analysis was 3-4 weeks after the last tamoxifen treatment. Tamoxifen efficacy was checked by enumerating blood naïve T cells in the case of *Spns2*$^{f/f}$*UBC*-CreERT2, where we saw naïve T cells in blood decline ~20-fold. In the case of *S1pr1*$^{f/f}$*UBC*-CreERT2, tamoxifen efficacy was checked by measuring surface S1PR1 or surface CD69 by flow cytometry, and deletion efficiency was 80-95%. We excluded experiments where deletion was less than 75%. We did not exclude non-deleted cells from analysis except when we sorted cells; this reduced the magnitude of differences, but avoided assumptions.

Bone marrow chimera generation: Recipients were lethally irradiated with two 5 Gy doses of x-ray irradiation separated by 3h, and received 2×10^6 bone marrow cells intravenously. Chimeras were analyzed at least 8 weeks after transplantation.

IL-7Rα blockade: Mice received 0.4mg anti-IL-7Rα (BioXCell) or isotype control (Rat IgG2a) intraperitoneally every 4 days for three total treatments.

Transfers of Bax$^{-/-}$ *or littermate control T cells*: T cells were isolated by negative selection using biotinylated antibodies against CD11b, CD11c, CD19, CD25, NK1.1, TCRγδ, and Ter119 and Magnisort Negative selection beads (Thermo Fisher Scientific) according to manufacturer's instructions, then labelled with CellTraceViolet or CellTraceYellow (Thermo Fisher Scientific). Dyes were swapped between genotypes between experiments. 1×10^6–2×10^6 T cells per group were transferred via retro-orbital injection.

4-deoxypyridoxine-HCl (DOP): Mice received 10 g/l sucrose plus 30 mg/l DOP (Sigma-Aldrich) or 10 g/l sucrose alone in drinking water for three weeks.

SEW-2871 (Cayman Chemical) was dissolved in ethanol at 9mg/mL as stock solution. Stock was diluted in vehicle of 50% Tween 20- 50%PBS. Solution was sonicated in a water bath for 10 minutes, then injected intraperitoneally at 10mg/kg daily.

H-89: 40mg/kg H-89 (Selleckchem) was given by gavage in vehicle of 5% DMSO, 30% PEG400, 1% Tween80, 64% PBS daily for 12d.

Dexamethasone (Sigma-Aldrich) was injected intraperitoneally in vehicle of PBS at 2mg/kg.

Irradiation: Adult (8-12 weeks) C57BL/6J mice were exposed to 1 Gy x-ray radiation.

ABT-199: 60mg/kg ABT-199 (Selleckchem) was given by gavage in vehicle of 8% DMSO, 45% PEG400, 5% Tween80, 42% PBS.

JNK inhibitors: 15mg/kg/day SP600125 (Selleckchem) or 20mg/kg/day JNK-IN-8 (MedChemExpress) was given intraperitoneally in vehicle of 4.5% DMSO, 40% PEG400, 5% Tween80, and 50.5% PBS daily for 12 days.

FTY720: Mice were injected intraperitoneally with 1mg/kg FTY720 (Cayman Chemical) in vehicle of 0.5% DMSO, 4.5% 2-hydroxypropyl-b-cyclodextrin and 95% PBS every other day for three weeks or as indicated.

SRBCs (Colorado Serum Company) were washed three times in PBS. Washed SRBCs were enumerated using Beckman Coulter Multisizer 3 and resuspended at 10^8 in 30μL. 10^8 SRBCs were subcutaneously injected into the left footpad, which drains to the popliteal and inguinal LN.

Cell preparation

For analysis by flow cytometry, lymphocytes were isolated from spleen or LN by mechanical disruption and filtration through a 70-μm cell strainer in isolation buffer (PBS with 2% FBS, 1mM EDTA). LN were combined cervical, brachial, axillary, inguinal and mesenteric, unless otherwise indicated. Lymphocytes were enumerated with a cell counter (Beckman Coulter Multisizer 3) set to detect nuclei between 3.5 and 10 μm. For adoptive transfer, T cells were purified by magnetic bead enrichment (Thermo Fisher Scientific) and retro-orbitally injected.

For CellTrace dye labeling, cells were resuspended at 20 x 10^6/mL in PBS and dyes were added to a final concentration of 5uM. Cells were incubated for 10 minutes at room temperature and the reaction was stopped by adding PBS-FBS to a final concentration of 20% FBS. Labeled cells were washed twice in PBS before injecting into mice.

To generate bone marrow chimeras, bone marrow cells were flushed from long bones of the leg. RBC were lysed using ACK lysis buffer (Gibco). Cells were resuspended at concentration of $2x10^6$/100μL PBS.

For human cells, PBMCs were isolated using Lymphoprep (StemCell Technologies) and Sepmate-50 (IVD) tubes (StemCell Technologies), according to manufacturer's instructions.

In vitro culture with ABT-199 and Fas ligand

Lymphocytes were treated either with ABT-199 (Tocris) or Fas ligand + Enhancer (Enzo Life Sciences) for 4h in a 37ºC 5% CO2 incubator. After 4h, cells were stained for surface markers and then stained for AnnexinV (BioLegend) and Propidium Iodide in AnnexinV binding buffer (BioLegend) for 15 minutes at room temperature.

Flow cytometry

Staining for S1PR1 was done on ice in PBS with 0.05% sodium azide, 1 mM EDTA and 0.5% FBS. Cells (2E6 in 25 microliters) were stained for 90 min with anti-mouse S1PR1 (74.4 μg/ml; R&D Systems), washed twice in buffer, stained for 45 min with anti-rat IgG-biotin F(ab′)2 (9.5 μg/ml; Jackson Immunoresearch), washed twice in buffer, and stained with streptavidin-APC and other antibodies.

To stain for active-Caspase and AnnexinV, single-cell suspensions (2E6 cells in 25 microliters) were stained for surface markers with 10μM CaspACE FITC-VAD-FMK for 1 hour in PBS supplemented with 1 mM EDTA and 0.5% FBS on ice. Cells were washed once in previous buffer and once in AnnexinV Binding Buffer (Biolegend). Then cells were stained with 1:50 dilution AnnexinV (BioLegend) Pacific Blue or APC in AnnexinV Binding Buffer for 15 minutes at room temperature.

For intracellular staining, cells were first stained with Fixable Live/Dead Blue (Thermo Fisher Scientific) according to manufacturer's instructions. Then, cells were stained for surface markers on ice for 30 minutes. Cells were fixed using eBioscience FoxP3 Fixation/Permeabilization kit for either 1 hour or overnight at 4ºC, then stained for intracellular markers for 1 hour. If secondary antibodies were required, this step was performed for 30 minutes.

For phospho-staining, tissues were mechanically disrupted in PBS to create a single cell suspension and immediately fixed in equal volume of 4% PFA for 15 minutes. Cells were washed in PBS with 2% FBS and 1mM EDTA, then stained for

surface markers [CD4 BUV395 (RM4-5), CD8 PE (5.3-6.7), CD62L BV421 (MEL-14), CD44 FITC (IM7), and CD25 BV650 (PC61)]. After surface staining, cells were permeabilized using eBioscience FoxP3 permeabilization kit for 1 hour. Cells were stained for phospho-antigens for 1 hour with primary antibodies and then stained using secondary antibodies for 30 minutes.

Flow cytometry data were acquired on an LSR-II flow cytometer (Becton Dickinson) and analyzed using FlowJo v10 software.

RNA isolation and sequencing

RNA was isolated from FACS-sorted naïve CD4+ T cells using TRIzol LS (Invitrogen) followed by DNase I (QIAGEN) treatment and cleanup with an Rneasy Plus Micro kit (QIAGEN), and quantified on a 2100 BioAnalyzer instrument (Agilent Technologies, Inc.). RNASeq library prep and sequencing were performed at the NYU Langone Genome Technology Center. 5-20 ngs total RNA was used to prepare libraries using Trio RNA-Seq library prep kit (Tecan Genomics, Inc.) following manufacturer's instructions. The protocol contains the following steps: DNase treatment to remove any DNA in the sample, first strand and second stand cDNA synthesis from the input RNA, single primer isothermal amplification (SPIA) of the resultant cDNAs, enzymatic fragmentation and construction of unique barcoded libraries, PCR library amplification (4 cycles were used) and an AnyDeplete step to remove rRNA transcripts. The Agencourt AMPure XP bead (Beckman Coulter) purified libraries were quantified using by qPCR and the size distribution was checked using Agilent TapeStation 2200 system. The libraries were subjected to paired-end 50 bp sequencing on NovaSeq 6000 sequencer (Illumina).

Sequencing reads were mapped to the mouse reference genome (GRCm38.85/mm10) using the STAR aligner (v2.5.0c). Alignments were guided by a Gene Transfer Format file. Mean read insert sizes and their standard deviations were calculated using Picard tools (v.1.126) (http://broadinstitute.github.io/picard). Read count tables were generated using HTSeq (v0.6.0), normalized based on their library size factors using DEseq2, and differential expression analysis was performed. Read per million normalized BigWig files were generated using BEDTools (v2.17.0) and bedGraphToBigWig tool (v4).

Recombinant DNA and retroviral transduction of T cells

For overexpression of S1PR1 mutants, cDNAs (synthesized by GenScript) were cloned into the retroviral plasmid MIGR1. MIGR1 was a gift from Warren Pear (Addgene plasmid #27490). Mutations in ST10A were alanine substitutions for S336, S351, S353, S355, S358, S359, T371, S374, S375, and S380. Plat-E cells, transfected with the constructs using Lipofectamine 2000 (Thermo Fisher Scientific), were used to produce retrovirus. Before retroviral transduction, naïve T cells from *S1pr1*Δ LN were isolated by negative selection using biotinylated antibodies against CD11b, CD11c, CD19, CD25, NK1.1, TCRγδ, and Ter119 and Magnisort Negative selection beads (Thermo Fisher Scientific) according to manufacturer's instructions. The cells were activated using anti-CD3ε and anti-CD28 cross-linking with 10 ng/mL IL2. T cells were transduced with virus at 24h and 40h post-activation. For transduction, cells were centrifuged at 30ºC 2500rpm for 90 mins in the presence of 4ug/mL polybrene (Sigma-Aldrich). 64h post-activation, T cells were removed from anti-CD3ε/anti-CD28 and IL-2 stimulation and changed to media containing 5ng/mL IL-7 and 10ng/mL IL-15 to generate T cells with central memory properties. T cells in IL-7 and IL-15 media were split 1:2 daily into new media containing IL-7 and IL-15, and cultured for a total of 3d. We did not sort cells before transfer. Instead, in analysis of recipient mice, we identified transferred cells using GFP (from the MIGR1 vector), and gated on cells with similar GFP expression for comparisons.

Transmission electron microscopy

FACS-sorted naïve CD4+ T cells from LNs and spleen were pelleted at 400g for 4 mins by swinging bucket Eppendorf 5810 into BEEM conical capsule tips (EMS, #69913-05), and fixed in 2% glutaraldehyde and 2% paraformaldehyde in 0.1M sodium cacodylate buffer (CB, pH 7.2) overnight at 4°C. The sample was processed following rOTO method (69, 70). Briefly, after washing with 0.1M CB three times for 5 min each, the cells were post-fixed with 2% osmium tetroxide and 1.5% potassium ferrocyanide in 0.1M CB for 1.5 hours on ice. After five washes of 3 min each in ddH_2O at room temperature, cells were placed in a filtered solution of 1% thiocarbohydrazide (TCH, Electron Microscopy Sciences, EMS, PA) in ddH_2O for 20 min at room temperature to allow additional staining. Cells were washed five times in ddH_2O again on ice, and placed in 2% aqueous OsO_4 for an additional 40 min on ice. Finally, cells were washed an additional five times in ddH_2O on ice, and placed in 1% aqueous uranyl acetate at 4°C overnight. Cells were washed five times in ddH_2O at room temperature, and en bloc lead staining was performed to enhance membrane contrast as follows. A lead aspartate solution

was made by dissolving 0.066 g of lead nitrate in 10 ml of 0.003 M aspartic acid. The pH was adjusted to 5.5 with 1N KOH, and the solution was placed in a 60°C oven for 30 min. The lead aspartate solution was filtered, and cells were stained at 60°C for 30 min, then washed five times in ddH_2O at room temperature and dehydrated in a graded series of ice-cold ethanol solutions (30, 50, 70, 85, 95, 100, 100%; 10 min each). Cells were then washed in ice cold acetone two times for 10 min each, followed by two acetone washes of 10 min each at room temperature. Cells were infiltrated gradually with EMbed812 epoxy resin (EMS) at room temperature by placing in 50% resin/acetone for 4 h, and 70% resin/acetone overnight. Cells were embedded in fresh 100% resin, and placed in a 60°C oven for 72 h to allow resin polymerization. EMbed 812 resin recipe: 5 ml EMbed 812, 4 ml DDSA, 2 ml NMA, 0.3 ml BDMA. 70 nm sections were cut, mounted on 200 mesh copper grids, and imaged with Talos120C transmission electron microscope (Thermo Fisher Scientific) with Gatan (4k x 4k) OneView Camera (Gatan, Inc., Pleasanton, CA).

Mitochondrial morphological analysis

Mitochondrial numbers and cross-sectional surface area were obtained using ImageJ by manually tracing only clearly discernible outlines of mitochondria on TEM images. Approximately 25-30 whole cell images were taken per sample at the same magnification for each group within an experiment.

Statistics

Statistical analysis was performed using GraphPad Prism v9. Graphs show mean $\pm$ SEM. P-values were calculated using unpaired two-tailed Student's t test, one-way ANOVA with multiple comparisons, or Brown-Forsythe and Welch ANOVA with multiple comparisons test, as indicated.

Study approval

All animal experiments were performed in accordance with protocols approved by the New York University Grossman School of Medicine Institutional Animal Care and Use Committee. Peripheral blood was drawn from anonymous, adult patients and healthy controls under protocol: Mucosal immune profiling in patients with inflammatory bowel disease IRB #: S12-01137.

Data Availability:

Values for all data points in graphs are reported in the Supporting Data Values file. Further information and requests for resources and reagents should be directed to Susan Schwab (Susan.Schwab@nyulangone.org). RNA-Seq datasets are in the NIH Gene Expression Omnibus, GSE221482.

Author Contributions:

D.D. designed and performed experiments, and wrote the manuscript; V.M.H., Y.S.Z., and M.O. performed experiments; J.E.C. designed and performed experiments; J.A. provided patient samples; and S.R.S. designed experiments and edited the manuscript.

Acknowledgements:

We thank Dan Littman, Jason Cyster, and Samantha Lux for thoughtful comments on the manuscript; Jason Cyster (University of California San Francisco) for *Grk2*$^{f/-}$CD4-Cre and control bone marrow; Ramin Herati (NYU) for help analyzing human PBMC; and Alice Liang (NYU) for expert assistance in electron microscopy. This work was supported by NIH R01AI085166 (SRS); NIH R01AI123308 (SRS); NIH R01DK093668 (KC); NIH R01CA237264 (JEC); NIH K23DK124570 (JEA); a Blood Cancer Discoveries Grant from the Leukemia and Lymphoma Society, the Mark Foundation for Cancer Research and The Paul G. Allen Frontiers Group (SRS); a Senior Research Award from the Crohn's & Colitis Foundation (KC); a Clinical Investigator Research Award from the Crohn's and Colitis Foundation (JEA); a pilot grant from the Judith & Stewart Colton Center for Autoimmunity (JEA); a Vilcek MSTP Scholar Fellowship (DD); NIH 5T32AI100853 (DD); NIH T32AR069515 (DD); NIH T32HD007520 (MO); NIH F31AI154793 (MO); and NIH P30CA016087, partially supporting NYU's core microscopy, flow cytometry, and genomics facilities.

References:

1. Starr TK, Jameson SC, and Hogquist KA. Positive and negative selection of T cells. *Annual review of immunology.* 2003;21:139-76.
2. Ryan JA, Brunelle JK, and Letai A. Heightened mitochondrial priming is the basis for apoptotic hypersensitivity of CD4+ CD8+ thymocytes. *Proc Natl Acad Sci U S A.* 2010;107(29):12895-900.
3. Hildeman DA, et al. Molecular mechanisms of activated T cell death in vivo. *Curr Opin Immunol.* 2002;14(3):354-9.
4. Surh CD, and Sprent J. Homeostasis of naive and memory T cells. *Immunity.* 2008;29(6):848-62.
5. Takada K, and Jameson SC. Naive T cell homeostasis: from awareness of space to a sense of place. *Nature reviews Immunology.* 2009;9(12):823-32.
6. Baeyens AAL, and Schwab SR. Finding a Way Out: S1P Signaling and Immune Cell Migration. *Annual review of immunology.* 2020;38:759-84.
7. Mendoza A, et al. Lymphatic endothelial S1P promotes mitochondrial function and survival in naive T cells. *Nature.* 2017;546(7656):158-61.
8. Perez-Jeldres T, Alvarez-Lobos M, and Rivera-Nieves J. Targeting Sphingosine-1-Phosphate Signaling in Immune-Mediated Diseases: Beyond Multiple Sclerosis. *Drugs.* 2021;81(9):985-1002.
9. Sandborn WJ, et al. Ozanimod as Induction and Maintenance Therapy for Ulcerative Colitis. *The New England journal of medicine.* 2021;385(14):1280-91.
10. Etemadifar M, et al. Multiple sclerosis disease-modifying therapies and COVID-19 vaccines: a practical review and meta-analysis. *Journal of neurology, neurosurgery, and psychiatry.* 2022.
11. Sabatino JJ, Jr., et al. Multiple sclerosis therapies differentially affect SARS-CoV-2 vaccine-induced antibody and T cell immunity and function. *JCI Insight.* 2022;7(4).
12. Sabatino JJ, et al. Longitudinal adaptive immune responses following sequential SARS-CoV-2 vaccinations in MS patients on anti-CD20 therapies and sphingosine-1-phosphate receptor modulators. *Mult Scler Relat Disord.* 2022;70:104484.
13. Ghadiri M, et al. Reconstitution of the peripheral immune repertoire following withdrawal of fingolimod. *Mult Scler.* 2017;23(9):1225-32.
14. Nagy S, Kuhle J, and Derfuss T. Lymphocyte recovery after fingolimod discontinuation in patients with MS. *Neurol Neuroimmunol Neuroinflamm.* 2020;7(6).
15. Ruzankina Y, et al. Deletion of the developmentally essential gene ATR in adult mice leads to age-related phenotypes and stem cell loss. *Cell Stem Cell.* 2007;1(1):113-26.
16. Pham TH, et al. Lymphatic endothelial cell sphingosine kinase activity is required for lymphocyte egress and lymphatic patterning. *The Journal of experimental medicine.* 2010;207(1):17-27, S1-4.
17. Liu CH, et al. Ligand-induced trafficking of the sphingosine-1-phosphate receptor EDG-1. *Mol Biol Cell.* 1999;10(4):1179-90.
18. Schwab SR, et al. Lymphocyte sequestration through S1P lyase inhibition and disruption of S1P gradients. *Science.* 2005;309(5741):1735-9.
19. Strub GM, et al. Extracellular and intracellular actions of sphingosine-1-phosphate. *Adv Exp Med Biol.* 2010;688:141-55.
20. Sun K, et al. Sphingosine-1-phosphate promotes erythrocyte glycolysis and oxygen release for adaptation to high-altitude hypoxia. *Nat Commun.* 2016;7:12086.
21. Strub GM, et al. Sphingosine-1-phosphate produced by sphingosine kinase 2 in mitochondria interacts with prohibitin 2 to regulate complex IV assembly and respiration. *FASEB J.* 2011;25(2):600-12.
22. Kim S, and Sieburth D. Sphingosine Kinase Activates the Mitochondrial Unfolded Protein Response and Is Targeted to Mitochondria by Stress. *Cell Rep.* 2018;24(11):2932-45.e4.
23. Sanna MG, et al. Sphingosine 1-phosphate (S1P) receptor subtypes S1P1 and S1P3, respectively, regulate lymphocyte recirculation and heart rate. *The Journal of biological chemistry.* 2004;279(14):13839-48.

24. Lee MJ, Evans M, and Hla T. The inducible G protein-coupled receptor edg-1 signals via the G(i)/mitogen-activated protein kinase pathway. *The Journal of biological chemistry.* 1996;271(19):11272-9.
25. Lee MJ, et al. Sphingosine-1-phosphate as a ligand for the G protein-coupled receptor EDG-1. *Science.* 1998;279(5356):1552-5.
26. Robertson TF, et al. Lymphocyte egress signal sphingosine-1-phosphate promotes ERM-guided, bleb-based migration. *The Journal of cell biology.* 2021;220(6).
27. Shaywitz AJ, and Greenberg ME. CREB: a stimulus-induced transcription factor activated by a diverse array of extracellular signals. *Annual review of biochemistry.* 1999;68:821-61.
28. Chijiwa T, et al. Inhibition of forskolin-induced neurite outgrowth and protein phosphorylation by a newly synthesized selective inhibitor of cyclic AMP-dependent protein kinase, N-[2-(p-bromocinnamylamino)ethyl]-5-isoquinolinesulfonamide (H-89), of PC12D pheochromocytoma cells. *The Journal of biological chemistry.* 1990;265(9):5267-72.
29. Souers AJ, et al. ABT-199, a potent and selective BCL-2 inhibitor, achieves antitumor activity while sparing platelets. *Nature medicine.* 2013;19(2):202-8.
30. Knudson CM, et al. Bax-deficient mice with lymphoid hyperplasia and male germ cell death. *Science.* 1995;270(5233):96-9.
31. Dhanasekaran DN, and Reddy EP. JNK signaling in apoptosis. *Oncogene.* 2008;27(48):6245-51.
32. Hotamisligil GS, and Davis RJ. Cell Signaling and Stress Responses. *Cold Spring Harb Perspect Biol.* 2016;8(10).
33. Bennett BL, et al. SP600125, an anthrapyrazolone inhibitor of Jun N-terminal kinase. *Proceedings of the National Academy of Sciences of the United States of America.* 2001;98(24):13681-6.
34. Zhang T, et al. Discovery of potent and selective covalent inhibitors of JNK. *Chemistry & biology.* 2012;19(1):140-54.
35. Lo CG, et al. Cyclical modulation of sphingosine-1-phosphate receptor 1 surface expression during lymphocyte recirculation and relationship to lymphoid organ transit. *The Journal of experimental medicine.* 2005;201(2):291-301.
36. Watterson KR, et al. Dual regulation of EDG1/S1P(1) receptor phosphorylation and internalization by protein kinase C and G-protein-coupled receptor kinase 2. *J Biol Chem.* 2002;277(8):5767-77.
37. Arnon TI, et al. GRK2-dependent S1PR1 desensitization is required for lymphocytes to overcome their attraction to blood. *Science.* 2011;333(6051):1898-903.
38. Thangada S, et al. Cell-surface residence of sphingosine 1-phosphate receptor 1 on lymphocytes determines lymphocyte egress kinetics. *The Journal of experimental medicine.* 2010;207(7):1475-83.
39. Manjunath N, et al. Effector differentiation is not prerequisite for generation of memory cytotoxic T lymphocytes. *The Journal of clinical investigation.* 2001;108(6):871-8.
40. Oo ML, et al. Immunosuppressive and anti-angiogenic sphingosine 1-phosphate receptor-1 agonists induce ubiquitinylation and proteasomal degradation of the receptor. *The Journal of biological chemistry.* 2007;282(12):9082-9.
41. Wu X, et al. Response of COVID-19 vaccination in multiple sclerosis patients following disease-modifying therapies: A meta-analysis. *EBioMedicine.* 2022;81:104102.
42. Saggau C, et al. The pre-exposure SARS-CoV-2-specific T cell repertoire determines the quality of the immune response to vaccination. *Immunity.* 2022.
43. Brinkmann V, and Lynch KR. FTY720: targeting G-protein-coupled receptors for sphingosine 1-phosphate in transplantation and autoimmunity. *Curr Opin Immunol.* 2002;14(5):569-75.
44. Mandala S, et al. Alteration of lymphocyte trafficking by sphingosine-1-phosphate receptor agonists. *Science.* 2002;296(5566):346-9.
45. Hataye J, et al. Naive and memory CD4+ T cell survival controlled by clonal abundance. *Science.* 2006;312(5770):114-6.

46. Don AS, et al. Essential requirement for sphingosine kinase 2 in a sphingolipid apoptosis pathway activated by FTY720 analogues. *J Biol Chem.* 2007;282(21):15833-42.
47. Nagahara Y, Ikekita M, and Shinomiya T. Immunosuppressant FTY720 induces apoptosis by direct induction of permeability transition and release of cytochrome c from mitochondria. *J Immunol.* 2000;165(6):3250-9.
48. Nagahara Y, Ikekita M, and Shinomiya T. T cell selective apoptosis by a novel immunosuppressant, FTY720, is closely regulated with Bcl-2. *Br J Pharmacol.* 2002;137(7):953-62.
49. Matsuda S, et al. Differential activation of c-Jun NH2-terminal kinase and p38 pathways during FTY720-induced apoptosis of T lymphocytes that is suppressed by the extracellular signal-regulated kinase pathway. *J Immunol.* 1999;162(6):3321-6.
50. Lee MJ, et al. Vascular endothelial cell adherens junction assembly and morphogenesis induced by sphingosine-1-phosphate. *Cell.* 1999;99(3):301-12.
51. Cuvillier O, et al. Suppression of ceramide-mediated programmed cell death by sphingosine-1-phosphate. *Nature.* 1996;381(6585):800-3.
52. Crilly SE, and Puthenveedu MA. Compartmentalized GPCR Signaling from Intracellular Membranes. *J Membr Biol.* 2021;254(3):259-71.
53. Wyant GA, et al. Mitochondrial remodeling and ischemic protection by G protein-coupled receptor 35 agonists. *Science.* 2022;377(6606):621-9.
54. McDonald PH, et al. Beta-arrestin 2: a receptor-regulated MAPK scaffold for the activation of JNK3. *Science.* 2000;290(5496):1574-7.
55. Reiter E, and Lefkowitz RJ. GRKs and beta-arrestins: roles in receptor silencing, trafficking and signaling. *Trends Endocrinol Metab.* 2006;17(4):159-65.
56. Benoit B, Baillet A, and Pous C. Cytoskeleton and Associated Proteins: Pleiotropic JNK Substrates and Regulators. *Int J Mol Sci.* 2021;22(16).
57. Parameswaran N, et al. Spatial coupling of JNK activation to the B cell antigen receptor by tyrosine-phosphorylated ezrin. *Journal of immunology.* 2013;190(5):2017-26.
58. Zhang Q, et al. DOCK8 regulates lymphocyte shape integrity for skin antiviral immunity. *The Journal of experimental medicine.* 2014;211(13):2549-66.
59. Foger N, et al. Requirement for coronin 1 in T lymphocyte trafficking and cellular homeostasis. *Science.* 2006;313(5788):839-42.
60. Shiow LR, et al. The actin regulator coronin 1A is mutant in a thymic egress-deficient mouse strain and in a patient with severe combined immunodeficiency. *Nature immunology.* 2008;9(11):1307-15.
61. Mendoza A, et al. The transporter Spns2 is required for secretion of lymph but not plasma sphingosine-1-phosphate. *Cell Rep.* 2012;2(5):1104-10.
62. Allende ML, Yamashita T, and Proia RL. G-protein-coupled receptor S1P1 acts within endothelial cells to regulate vascular maturation. *Blood.* 2003;102(10):3665-7.
63. Madsen L, et al. Mice lacking all conventional MHC class II genes. *Proc Natl Acad Sci U S A.* 1999;96(18):10338-43.
64. Murata K, et al. CD69-null mice protected from arthritis induced with anti-type II collagen antibodies. *International immunology.* 2003;15(8):987-92.
65. Pappu R, et al. Promotion of lymphocyte egress into blood and lymph by distinct sources of sphingosine-1-phosphate. *Science.* 2007;316(5822):295-8.
66. Mizugishi K, et al. Essential role for sphingosine kinases in neural and vascular development. *Mol Cell Biol.* 2005;25(24):11113-21.
67. Hogquist KA, et al. T cell receptor antagonist peptides induce positive selection. *Cell.* 1994;76(1):17-27.
68. Barnden MJ, et al. Defective TCR expression in transgenic mice constructed using cDNA-based alpha- and beta-chain genes under the control of heterologous regulatory elements. *Immunol Cell Biol.* 1998;76(1):34-40.

69. Liang F-X, et al. Challenges Facing an EM Core Laboratory: Mitochondria Structural Preservation and 3DEM Data Presentation. *Microscopy Today.* 2021;29(1):18-23.
70. Wilke SA, et al. Deconstructing complexity: serial block-face electron microscopic analysis of the hippocampal mossy fiber synapse. *J Neurosci.* 2013;33(2):507-22.
71. Shiow LR, et al. CD69 acts downstream of interferon-alpha/beta to inhibit S1P1 and lymphocyte egress from lymphoid organs. *Nature.* 2006;440(7083):540-4.

Figure 1: SPNS2-derived S1P and S1PR1 prevent apoptotic death of naïve T cells

A-B) (A) *Spns2*$^{f/f}$ *UBC*-CreERT2 mice and littermate controls were treated with tamoxifen, and 3-4 weeks later LN T cells were analyzed by flow cytometry. (B) Frequency of active caspase (ActCasp)+ AnnexinV+ and propidium iodide (PI)+ cells among naïve CD4+ T cells. Compilation of 4 experiments, 8 mice/group.

C-E) (C) *Spns2*$^{f/f}$ *Lyve1*-Cre and littermate controls were treated with 10mg/kg SEW-2871 or vehicle daily. After ten days of treatment, LN T cells were analyzed by flow cytometry. (D) Representative histogram of S1PR1 expression on naïve CD4+ T cells from LN of *Spns2*Δ mice and littermate controls, with and without SEW-2871 treatment. (E) Frequency of ActCasp+ AnnexinV+ cells among naïve CD4+ T cells in LN of *Spns2*Δ mice and littermate controls, with and without SEW-2871 treatment. Compilation of 4 experiments, 4-6 mice/group.

F-G) (F) *S1pr1*$^{f/f}$ *UBC*-CreERT2 mice and littermate controls were treated with 10mg/kg SEW-2871 or vehicle daily for 12 days and treated with tamoxifen on d1 and d2. On d12, LN cells were analyzed by flow cytometry. (G) Frequency of ActCasp+ AnnexinV+ cells among naïve CD4+ T cells in LN of *S1pr1*Δ mice and littermate controls, with and without SEW-2871 treatment. Compilation of 4 experiments with n=4-5 mice per group.

B, Student's t test. E,G, One-way ANOVA with multiple comparisons. *p≤0.05, **p≤0.01, ***p≤0.001, ****p≤0.0001, ns non-significant.

Figure 2: Canonical S1PR1 signaling pathways do not regulate naïve T cell survival.

A-B) pAKT T308 measured by flow cytometry. (A) Representative histogram of pAKT T308 in naïve CD4+ T cells from the skin-draining LN of (left) a *Spns2*$^{f/f}$*Lyve1*-Cre mouse and littermate control, or (right) a *S1pr1*$^{f/f}$*UBC*-CreERT2 mouse and littermate control 3-4 weeks after tamoxifen treatment. pAKT T308 in WT CD4 T cells activated in vitro served as a comparison (same comparison used in both plots). (B) Compilation. Each point represents the ratio of the pAKT T308 geometric mean fluorescence intensity (MFI) in naïve CD4 T cells from a *Spns2*Δ mouse to the pAKT T308 MFI in naïve CD4 T cells from its littermate control, or the ratio of the pAKT T308 MFI in naïve CD4 T cells from a *S1pr1*Δ mouse to the pAKT T308 MFI in naïve CD4 T cells from its littermate control. skinLN, skin-draining LN. mesLN, mesenteric LN. Compilation of 4 experiments with 4 pairs of mice for *Spns2* and 8 experiments with 8 pairs for *S1pr1*.

(C) As in (B), for pERK.

D-E) Phosphorylated CREB (pCREB) measured by flow cytometry. (D) Representative histogram of pCREB in naïve CD4+ T cells from LN of (left) a *Spns2*$^{f/f}$ *Lyve1*-Cre mouse and littermate control, or (right) a *S1pr1*$^{f/f}$ *UBC*-CreERT2 mouse and littermate control 3-4 weeks after tamoxifen treatment. (E) As in (B), for pCREB. Compilation of 2-3 experiments with 2-3/group.

F-H) (F) Experiment design. (G) Relative pCREB expression in naïve CD4+ T cells. Each point represents the MFI in one individual mouse divided by the mean MFI in vehicle-treated control mice in that experiment. (H) Frequency of ActCasp+ AnnexinV+ cells among naïve CD4+ T cells in LN. Compilation of 3 experiments, with 4/group.

G,H one-way ANOVA with multiple comparisons. *p≤0.05, **p≤0.01, ns non-significant.

Figure 3: BCL-2 family proteins regulate S1PR1-dependent naïve T cell survival

Expression of BCL-2 family members by naïve CD4+ T cells from LN of *Spns2*Δ or *S1pr1*Δ mice and littermate controls, analyzed by flow cytometry. (A-B) Representative histogram from a *Spns2*$^{f/f}$ *Lyve1*-Cre mouse and its littermate control, and compilation of BCL-2 expression. Each point represents the ratio of BCL-2 MFI between a *Spns2*Δ or *S1pr1*Δ mouse and its littermate control (or the mean of littermate controls if there were more than one). Compilation of 5-6 experiments with n=5-7/group. (C-D) As in (A-B) for PUMA. Compilation of 5-6 experiments with n=5-6 pairs/group. (E-F) As in (A-B) for BAX. Compilation of 6 experiments with n=5-8 pairs/group. Student's t test, comparing (KO MFI)/(mean ctrl MFI) to (ctrl MFI)/(mean ctrl MFI). *p≤0.05, **p≤0.01, ***p≤0.001, ****p≤0.0001, ns non-significant.

Figure 4: BCL-2 family proteins regulate S1PR1-dependent naïve T cell survival

A-B) (A) *S1pr1*Δ and littermate control lymphocytes labeled with CellTraceViolet or CellTraceYellow (dyes swapped between experiments) were co-transferred (1:1 for naïve CD4 T cells) intravenously into WT recipients. 24h later, recipients were treated with ABT-199. 24h later, dye-labeled naïve CD4 T cells in LN were enumerated. (B) Ratio of the number of naïve CD4+ T cells from *S1pr1*Δ donor vs control donor recovered in indicated recipients. Compilation of 3 experiments, 5-6/group.

C-E) Lymphocytes from LN of *S1pr1*Δ or littermate control mice were treated with indicated concentrations of (D) ABT-199 or (E) Fas ligand ex vivo for 4h. Frequency of AnnexinV+ PI+ cells among naïve CD4+ T cells measured by flow

cytometry. Each point represents mean of two technical replicates, minus mean frequency of AnnexinV+ PI+ cells in two vehicle-treated technical replicates. Compilation of 3 experiments, 4/group.

F-G) (F) Experiment design. (G) Relative BCL-2, PUMA, and BAX expression in naïve CD4+ T cells, shown as in Fig. 2F. Compilation of 4 experiments, n=5-8/group.

H-I) (H) *Bax*$^{-/-}$ and WT littermate control lymphocytes labeled with CellTraceViolet or CellTraceYellow (dyes swapped between experiments) were co-transferred (1:1 for naïve CD4 T cells) intravenously into *Spns2*Δ mice and littermate controls. 21d later, cells in skin-draining and mesenteric LN were enumerated. (I) Ratio of WT:*Bax*$^{-/-}$ naïve CD4 T cells in indicated mice. Compilation of 3 experiments, 6-8/group.

J) CellTraceViolet-labeled *Bax*$^{-/-}$ lymphocytes were transferred intravenously into *Spns2*$^{f/f}$ *Lyve1*-Cre mice or littermate controls. 21d later, dye-labeled LN naïve CD4+ T cells were analyzed by flow cytometry. Compilation of BCL-2 and PUMA expression by *Bax*$^{-/-}$ naïve T cells, as in Fig. 3. Compilation of 3 experiments, 3-6/group.

B,D-E,I: Student's t test. G: One-way ANOVA with multiple comparisons. *p≤0.05, **p≤0.01, ***p≤0.001, ns non-significant.

Figure 5: JNK signaling regulates S1P-dependent naïve T cell survival

(A) Representative histogram from a *Spns2*$^{f/f}$ *Lyve1*-Cre mouse and littermate control, and compilation of pJNK expression. Each point represents the ratio of pJNK MFI between a *Spns2*Δ or *S1pr1*Δ mouse and its littermate control (or mean of littermate controls, if more than one). Compilation of 4-5 experiments, 5-6/group. (B) As in (A) for pcJUN. Compilation of 4-5 experiments, 5-6/group. (C) As in (A) for pMKK7. Compilation of 4 experiments, 4-5/group.

D-G) (D) Starting on d0, *S1pr1*$^{f/f}$*UBC*-CreERT2 and littermate control mice were treated daily with 15 mg/kg SP-600125 (filled circles) or 20 mg/kg JNK-IN-8 (open circles) or vehicle. On d1 and d2, the mice were treated with tamoxifen. On d12, naïve CD4+ T cells in LN were analyzed. Relative values represent expression in one mouse divided by the mean for vehicle-treated controls in that experiment. (E) Relative pcJUN expression. (F) Frequency of ActCasp+ AnnexinV+ among naïve CD4+ T cells. (G) Relative BCL-2, PUMA, and BAX expression. Compilation of 6 experiments (4: SP600125 ; 2: JNK-IN-8), 6-7/group.

(H) *Spns2*$^{f/f}$*UBC*-CreERT2 mice and littermate controls were treated with tamoxifen. 3 weeks later, mice were treated with 30mg/l DOP and 10mg/l sucrose, or sucrose alone, in drinking water. After 3 weeks of treatment, naïve CD4+ T cells in LN were stained for pJNK. Relative values as in (D). Compilation of 3 experiments, 3-5/group.

I) CellTraceViolet-labeled *Bax*$^{-/-}$ lymphocytes were transferred intravenously into *Spns2*$^{f/f}$Lyve1-Cre mice or littermate controls. 21d later, dye-labeled naïve CD4+ T cells in LN were analyzed by flow cytometry. Compilation of relative pJNK and pMKK7 expression by *Bax*$^{-/-}$ naïve T cells. Relative values represent the MFI in one mouse divided by the mean MFI for controls in that experiment. Compilation of 2 experiments, 4-5/group.

A-C,I: Student's t test. E-H, one-way ANOVA with multiple comparisons. *p≤0.05, **p≤0.01, ***p≤0.001, ****p≤0.0001.

Figure 6: GRK2 regulates naïve T cell survival

A-F) (A) CD45.1/2 WT mice were lethally irradiated and reconstituted with either *Grk2*$^{f/-}$*Cd4*-Cre (*Grk2*Δ) or *Grk2*$^{f/+}$*Cd4*-Cre (ctrl) bone marrow. 8-12 weeks after bone marrow transfer, naïve T cells were analyzed. (B, C) (B) Representative histogram of surface S1PR1 on naïve CD4+ T cells in blood, and (C) compilation. (D) Frequency of ActCasp+ AnnexinV+ cells among naïve CD4+ T cells in LN. (E) Relative MFI values for p-MKK7 and p-JNK and (F) for BCL-2, PUMA, and BAX. Relative values represent expression in one mouse divided by the mean for littermate controls in that experiment. Compilation of 4 experiments, 6-7/group. Student's t test. *p≤0.05, **p≤0.01, ***p≤0.001, ****p≤0.0001, ns non-significant.

Figure 7: Loss of S1PR1 internalization contributes to apoptosis

A-G) T cells were isolated from LN of *S1pr1*Δ mice; activated in vitro with anti-CD3/CD28; and retrovirally transduced with vector encoding either IRES-GFP (empty vector), WT S1PR1-IRES-GFP, or ST10A S1PR1-IRES-GFP. Transduced T cells were cultured for 3d in IL-7/IL-15 media to generate predominantly CD8+ 'central memory-like' T cells. These T cells were transferred into WT recipients and, 5d later, transferred CD8+ T cells were analyzed. (A) Schematic of ST10A. (B) Experiment design. (C-D) Representative histogram and compilation of relative surface S1PR1 expression on cells in blood and LN. Relative surface S1PR1 represents MFI on cells in one mouse divided by the mean MFI on WT S1PR1-transduced T cells in that experiment. (E) Absolute S1PR1 MFI values on the indicated cells. (F) Frequency of AnnexinV+ cells among CD8+ GFP+ T cells in LN. (G) Relative MFI for BCL-2 and p-JNK in CD8+ GFP+ T cells in LN. Relative

values represent expression in one mouse divided by the mean for WT S1PR1-transduced cells in that experiment. Compilation of 5 experiments, 5-6/group.

C-E, Student's t test. F-G, one-way ANOVA with multiple comparisons. *p≤0.05, **p≤0.01, ***p≤0.001, ns non-significant.

Figure 8: S1PR1 modulators impair T cell survival in mice and humans.

A-D) (A) WT mice were treated with 1mg/kg FTY720 or vehicle every other day for three weeks, and naïve CD4+ T cells in LN analyzed by flow cytometry. (B) Frequency ActCasp+AnnexinV+ and PI+ among naïve CD4+ T cells in LN. Compilation of 3 experiments, 9-10/group. (C) Relative MFI for pMKK7 and pJNK. Relative MFI represents MFI in one mouse divided by the mean for controls in that experiment. pMKK7: compilation of 2 experiments, 4-6/group. pJNK: compilation of 3 experiments, 6-9/group. (D) Relative MFI for BCL-2, PUMA, and BAX. Compilation of 3 experiments, 6-9/group.

E-H) (E) PBMCs were isolated from UC patients treated with ozanimod (UC+Oza), UC patients not treated with ozanimod (UC), or healthy controls (HC), and analyzed by flow cytometry. (F) Frequency AnnexinV+ among naïve CD4+ T cells. Compilation of 10 experiments, 8-11/group. (G) Representative histograms and compilations of pJNK and pMKK7 relative MFI for naïve CD4 T cells. Relative MFI represents MFI in one sample divided by the mean for the indicated comparison group on that day. Column 1: UC patients not treated with ozanimod compared to healthy controls. Column 2: UC patients treated with ozanimod compared to healthy controls. Column 3: UC patients treated with ozanimod compared to UC patients not treated with ozanimod. Each UC patient with ozanimod is represented once; if there was a choice between comparing that patient with a healthy control or a UC patient not taking ozanimod, the UC patient treated with ozanimod was compared to the UC patient not taking ozanimod. Compilation of 10 experiments, 3-7/group. (H) Representative histograms and compilation of relative MFI for BCL-2 and PUMA. Compilation of 10 experiments, 3-7/group.

B-D: Student's t test. F-H: one-way ANOVA with multiple comparisons. *p≤0.05, **p≤0.01, ***p≤0.001, ****p≤0.0001, ns non-significant.

Figure 9: Prolonged FTY720 treatment impairs germinal center responses.

A-D) (A) WT mice were divided into 3 groups. "Long FTY": 1mg/kg FTY720 every other day for 3 weeks (starting d -21). "Vehicle": vehicle for 3 weeks (starting d -21). "Short FTY": untreated until d -1, when received 1mg/kg FTY. On d0, all

mice received 10^8 SRBCs subcutaneously. FTY720 (long and short FTY720 groups) or vehicle (vehicle group) treatment continued until d8, when draining LN were analyzed. (B) Representative plots of GC B cells (Fas+CD38-), gated on B220+ B cells. Numbers represent percent GC of total B cells. (C) Number GC B or (D) T follicular helper cells in draining LN. Compilation of 3 experiments, 5-6/group.

E-G) (E) Three groups of WT mice were treated with FTY720 for three weeks. One group (Long FTY + polyclonal T cells) received CD4+ and CD8+ naive T cells from FTY720-treated WT mice (donor mice initiated FTY720 at the same time as recipient groups), either once (d -1: open circles) or three times (d -15, d -8, and d -1: closed circles). The second group received OVA-specific CD4+ and CD8+ T cells from FTY720-treated OTI and OTII transgenic mice (donor mice initiated FTY720 at the same time as recipient groups) three times (d -15, d -8, and d -1: closed circles); the ratio of OTI:OTII matched the ratio of CD8+:CD4+ T cells in the polyclonal transfer. One group received FTY720 at d -1 (Short FTY). On d0, all mice were received 10^8 SRBCs subcutaneously. FTY720 treatment continued in all groups until d8, when draining LN were analyzed. (F) Number GC B cells and (G) T follicular helper cells in draining LN. 4 experiments, 5-10/group.

C-D, one way ANOVA with multiple comparisons. F-G, Brown-Forsythe and Welch ANOVA test. *$p \leq 0.05$, **$p \leq 0.01$, ***$p \leq 0.001$, ****$p \leq 0.0001$, ns non-significant.

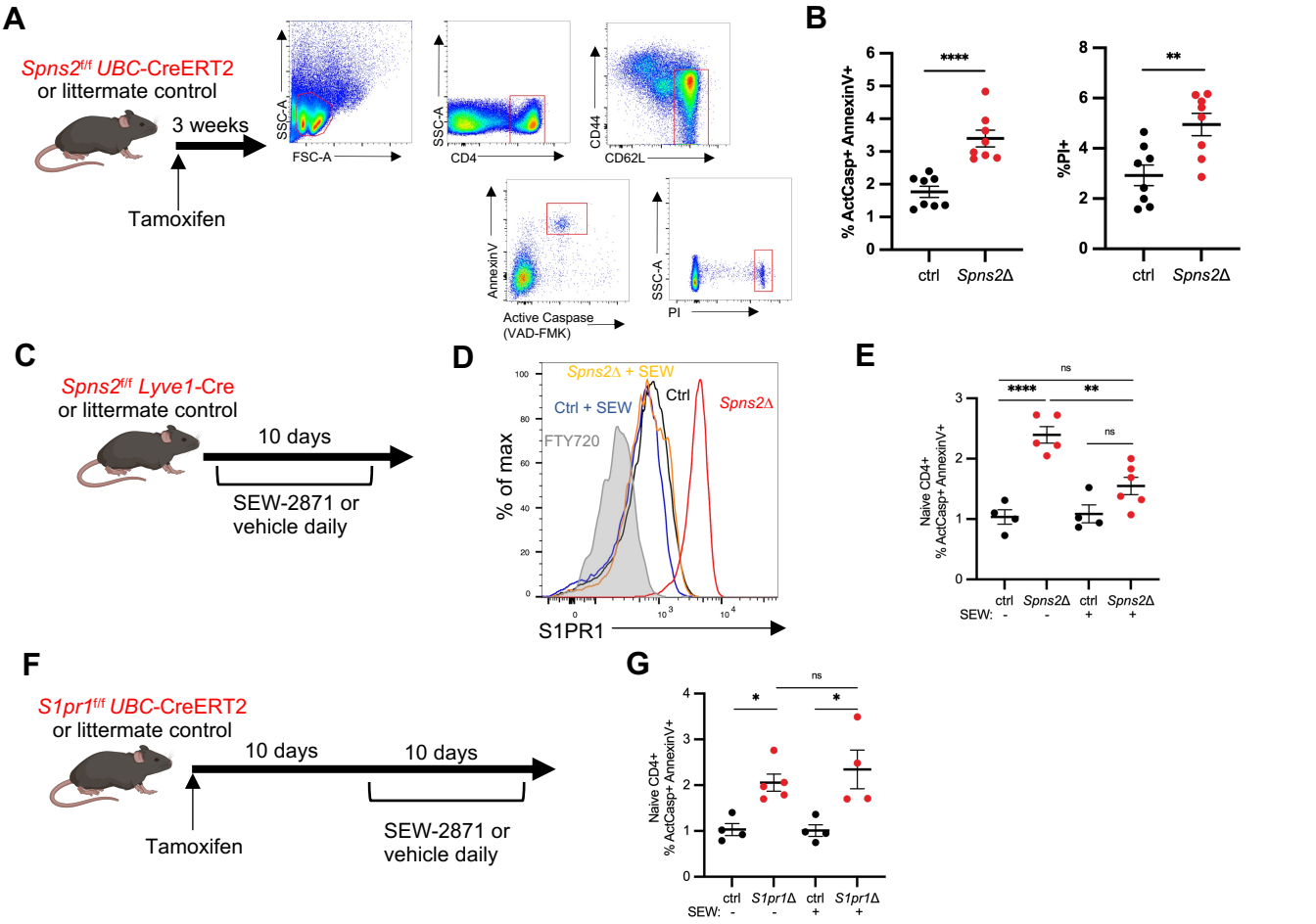
A
Spns2f/f UBC-CreERT2
or littermate control
3 weeks
Tamoxifen
SSC-A
FSC-A
SSC-A
CD4
CD44
CD62L
AnnexinV
Active Caspase
(VAD-FMK)
SSC-A
PI
B
% ActCasp+ AnnexinV+
****
ctrl
Spns2Δ
%PI+
**
ctrl
Spns2Δ
C
Spns2f/f Lyve1-Cre
or littermate control
10 days
SEW-2871 or
vehicle daily
D
Spns2Δ + SEW
Ctrl + SEW
FTY720
Ctrl
Spns2Δ
% of max
S1PR1
E
Naive CD4+
% ActCasp+ AnnexinV+
ns
****
**
ns
ctrl
Spns2Δ
ctrl
Spns2Δ
SEW: - - + +
F
S1pr1f/f UBC-CreERT2
or littermate control
10 days
10 days
Tamoxifen
SEW-2871 or
vehicle daily
G
Naive CD4+
% ActCasp+ AnnexinV+
ns
*
*
ctrl
S1pr1Δ
ctrl
S1pr1Δ
SEW: - - + +

Figure 1

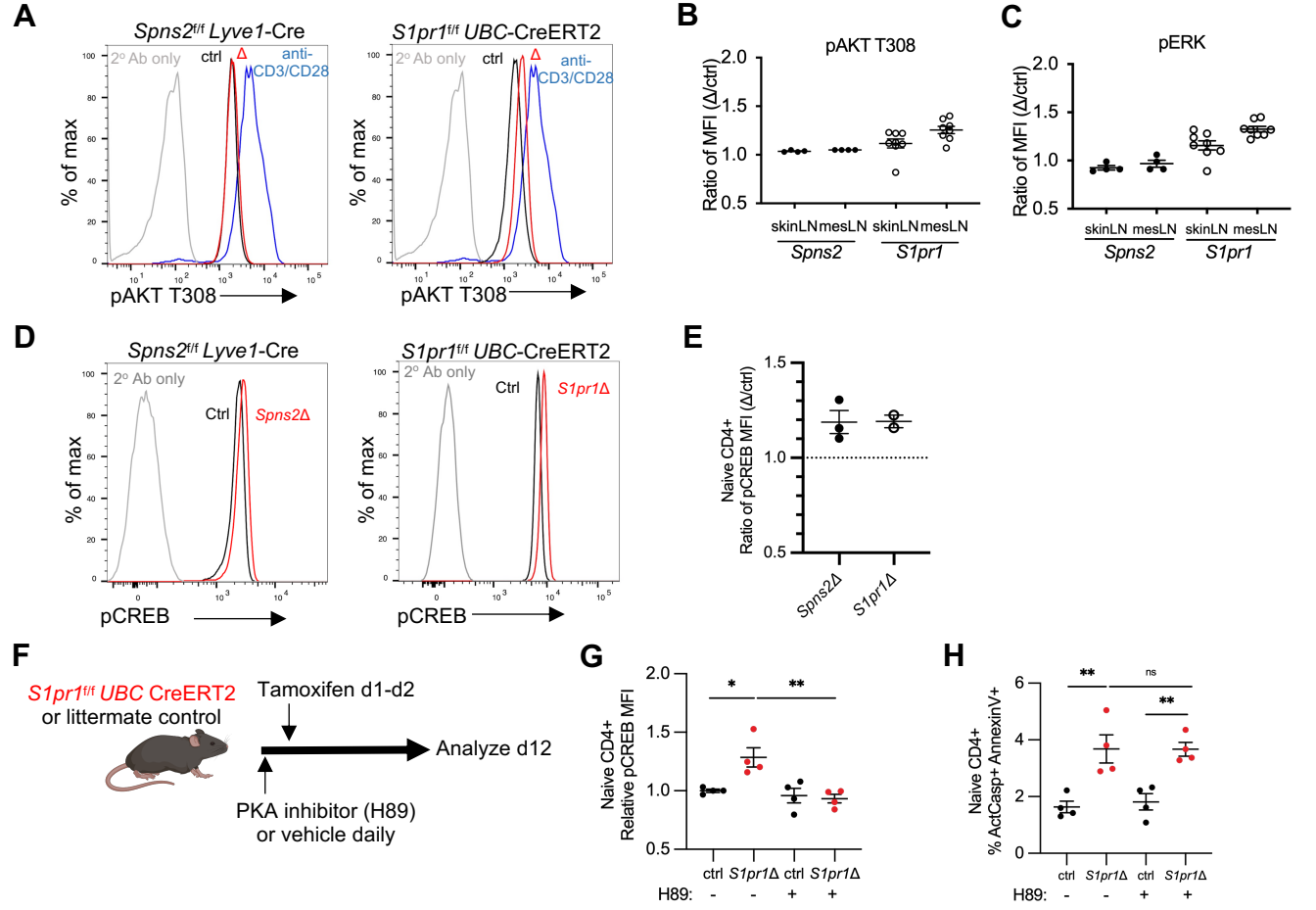
A
Spns2f/f Lyve1-Cre
S1pr1f/f UBC-CreERT2
2° Ab only
ctrl
anti-CD3/CD28
% of max
pAKT T308
B
pAKT T308
Ratio of MFI (Δ/ctrl)
skinLN mesLN skinLN mesLN
Spns2
S1pr1
C
pERK
D
Spns2f/f Lyve1-Cre
S1pr1f/f UBC-CreERT2
Ctrl
Spns2Δ
S1pr1Δ
pCREB
E
Naive CD4+
Ratio of pCREB MFI (Δ/ctrl)
F
S1pr1f/f UBC CreERT2
or littermate control
Tamoxifen d1-d2
Analyze d12
PKA inhibitor (H89)
or vehicle daily
G
Naive CD4+
Relative pCREB MFI
ctrl S1pr1Δ ctrl S1pr1Δ
H89: - - + +
H
Naive CD4+
% ActCasp+ AnnexinV+
ns

Figure 2

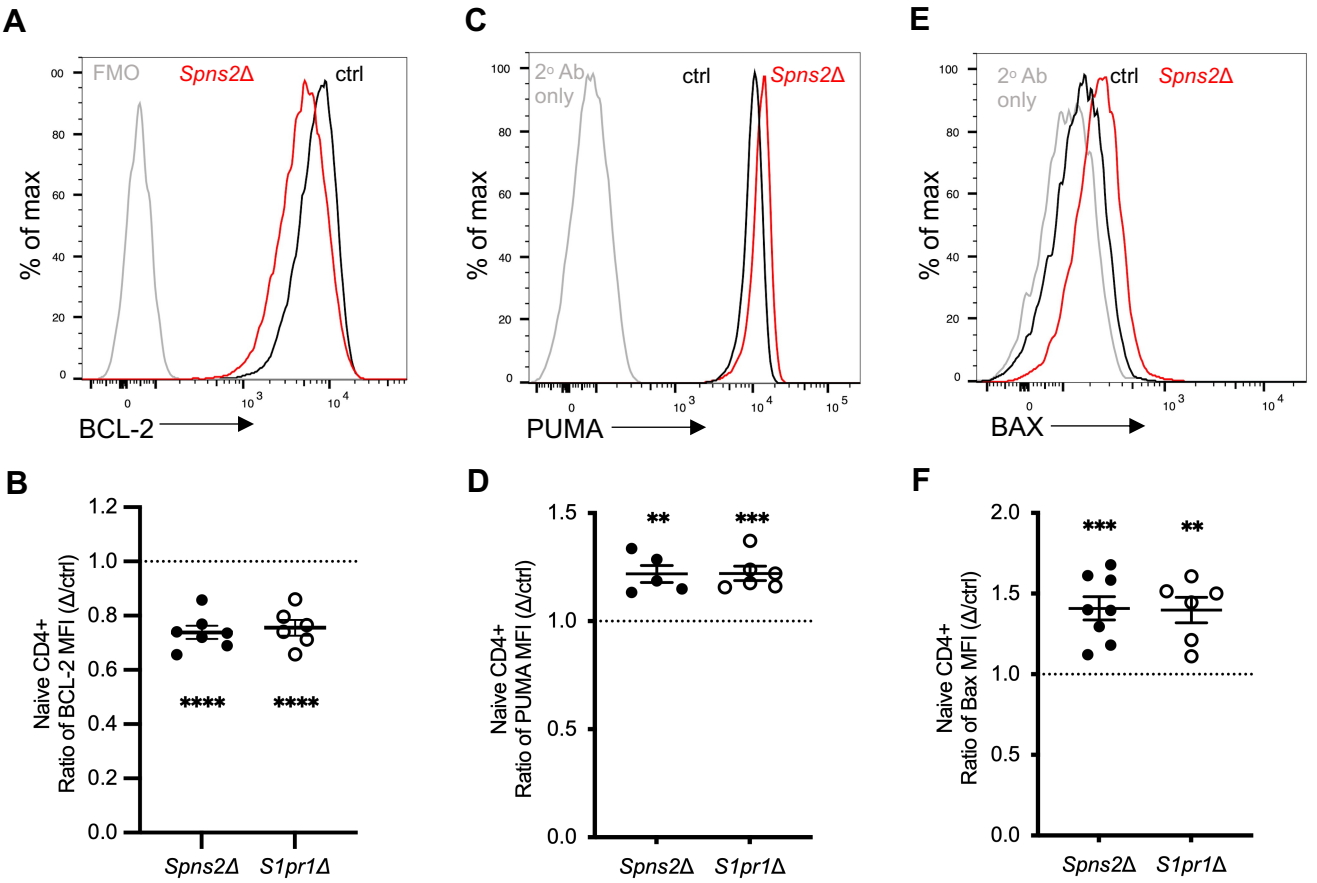
A
FMO
Spns2Δ
ctrl
% of max
BCL-2
C
2° Ab only
ctrl
Spns2Δ
% of max
PUMA
E
2° Ab only
ctrl
Spns2Δ
% of max
BAX
B
Naive CD4+ Ratio of BCL-2 MFI (Δ/ctrl)
****
****
Spns2Δ
S1pr1Δ
D
Naive CD4+ Ratio of PUMA MFI (Δ/ctrl)
**
***
Spns2Δ
S1pr1Δ
F
Naive CD4+ Ratio of Bax MFI (Δ/ctrl)
***
**
Spns2Δ
S1pr1Δ

Figure 3

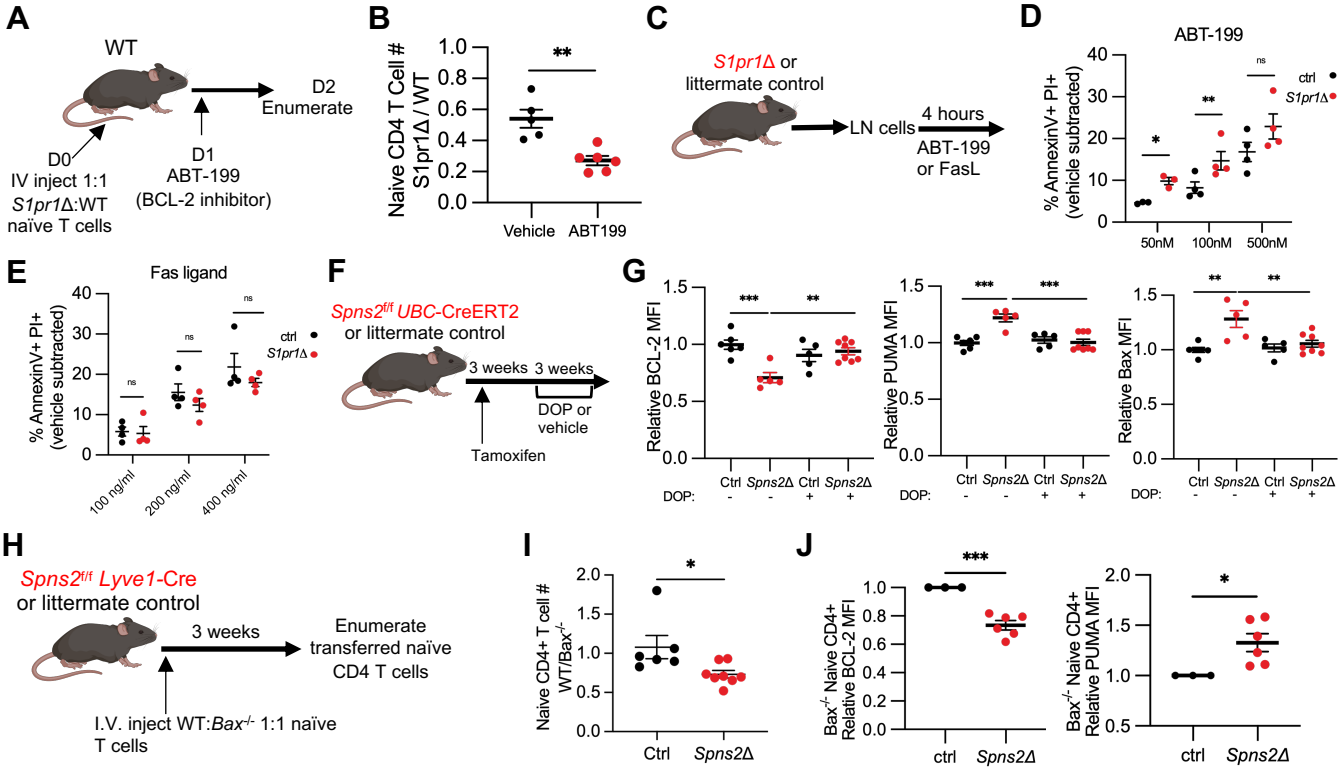
A
WT
D0
IV inject 1:1
S1pr1Δ:WT
naïve T cells
D1
ABT-199
(BCL-2 inhibitor)
D2
Enumerate
B
Naive CD4 T Cell #
S1pr1Δ / WT
Vehicle
ABT199
C
S1pr1Δ or
littermate control
LN cells
4 hours
ABT-199
or FasL
D
ABT-199
% AnnexinV+ PI+
(vehicle subtracted)
ctrl
S1pr1Δ
50nM
100nM
500nM
E
Fas ligand
% AnnexinV+ PI+
(vehicle subtracted)
ctrl
S1pr1Δ
100 ng/ml
200 ng/ml
400 ng/ml
F
Spns2f/f UBC-CreERT2
or littermate control
3 weeks
3 weeks
DOP or
vehicle
Tamoxifen
G
Relative BCL-2 MFI
Relative PUMA MFI
Relative Bax MFI
DOP:
Ctrl
Spns2Δ
H
Spns2f/f Lyve1-Cre
or littermate control
3 weeks
Enumerate
transferred naïve
CD4 T cells
I.V. inject WT:Bax-/- 1:1 naïve
T cells
I
Naive CD4+ T cell #
WT/Bax-/-
Ctrl
Spns2Δ
J
Bax-/- Naive CD4+
Relative BCL-2 MFI
Bax-/- Naive CD4+
Relative PUMA MFI
ctrl
Spns2Δ

Figure 4

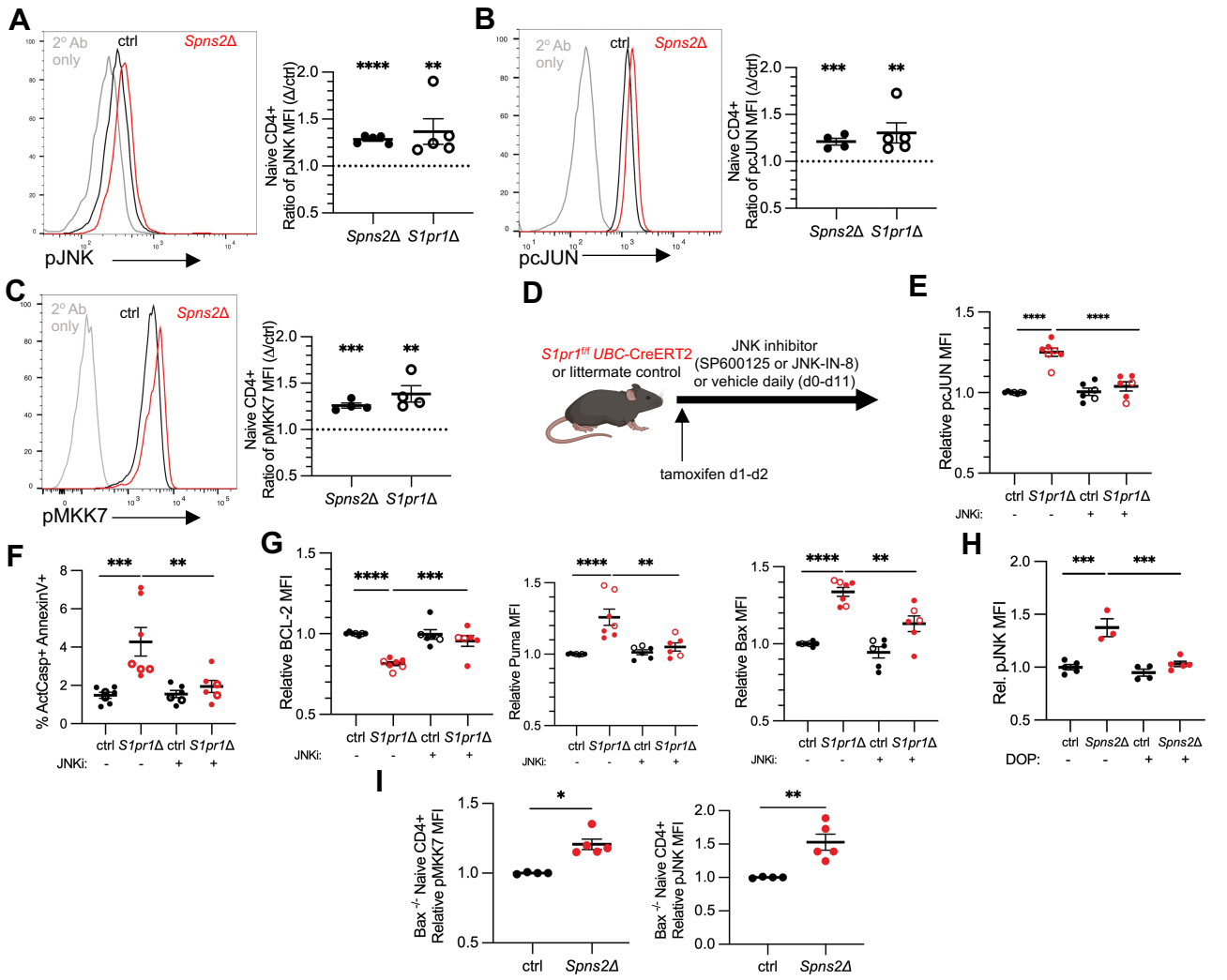
A
2° Ab only
ctrl
Spns2Δ
pJNK
Naive CD4+ Ratio of pJNK MFI (Δ/ctrl)
Spns2Δ S1pr1Δ
B
pcJUN
Naive CD4+ Ratio of pcJUN MFI (Δ/ctrl)
C
pMKK7
Naive CD4+ Ratio of pMKK7 MFI (Δ/ctrl)
D
S1pr1f/f UBC-CreERT2
or littermate control
JNK inhibitor
(SP600125 or JNK-IN-8)
or vehicle daily (d0-d11)
tamoxifen d1-d2
E
Relative pcJUN MFI
JNKi:
F
% ActCasp+ AnnexinV+
G
Relative BCL-2 MFI
Relative Puma MFI
Relative Bax MFI
H
Rel. pJNK MFI
DOP:
I
Bax-/- Naive CD4+ Relative pMKK7 MFI
Bax-/- Naive CD4+ Relative pJNK MFI

Figure 5

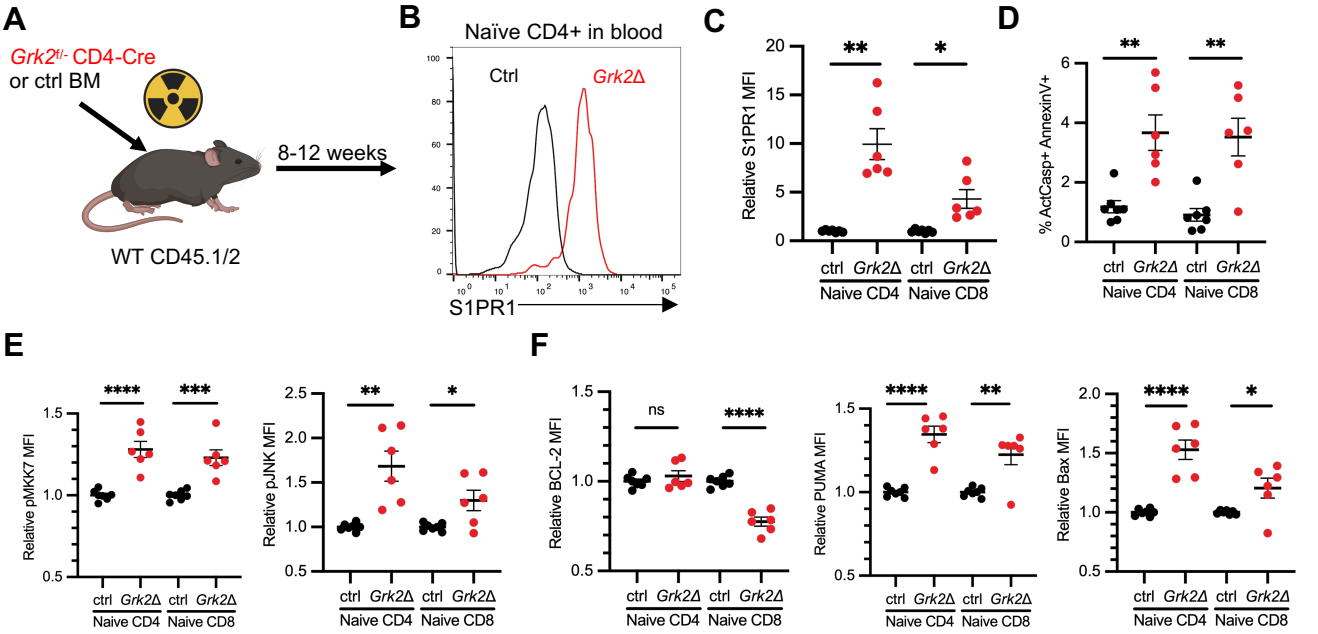
A
Grk2fl- CD4-Cre
or ctrl BM
8-12 weeks
WT CD45.1/2
B
Naïve CD4+ in blood
Ctrl
Grk2Δ
S1PR1
C
Relative S1PR1 MFI
**
*
ctrl Grk2Δ ctrl Grk2Δ
Naive CD4 Naive CD8
D
% ActCasp+ AnnexinV+
**
**
ctrl Grk2Δ ctrl Grk2Δ
Naive CD4 Naive CD8
E
Relative pMKK7 MFI
****
***
Relative pJNK MFI
**
*
F
Relative BCL-2 MFI
ns
****
Relative PUMA MFI
****
**
Relative Bax MFI
****
*

Figure 6

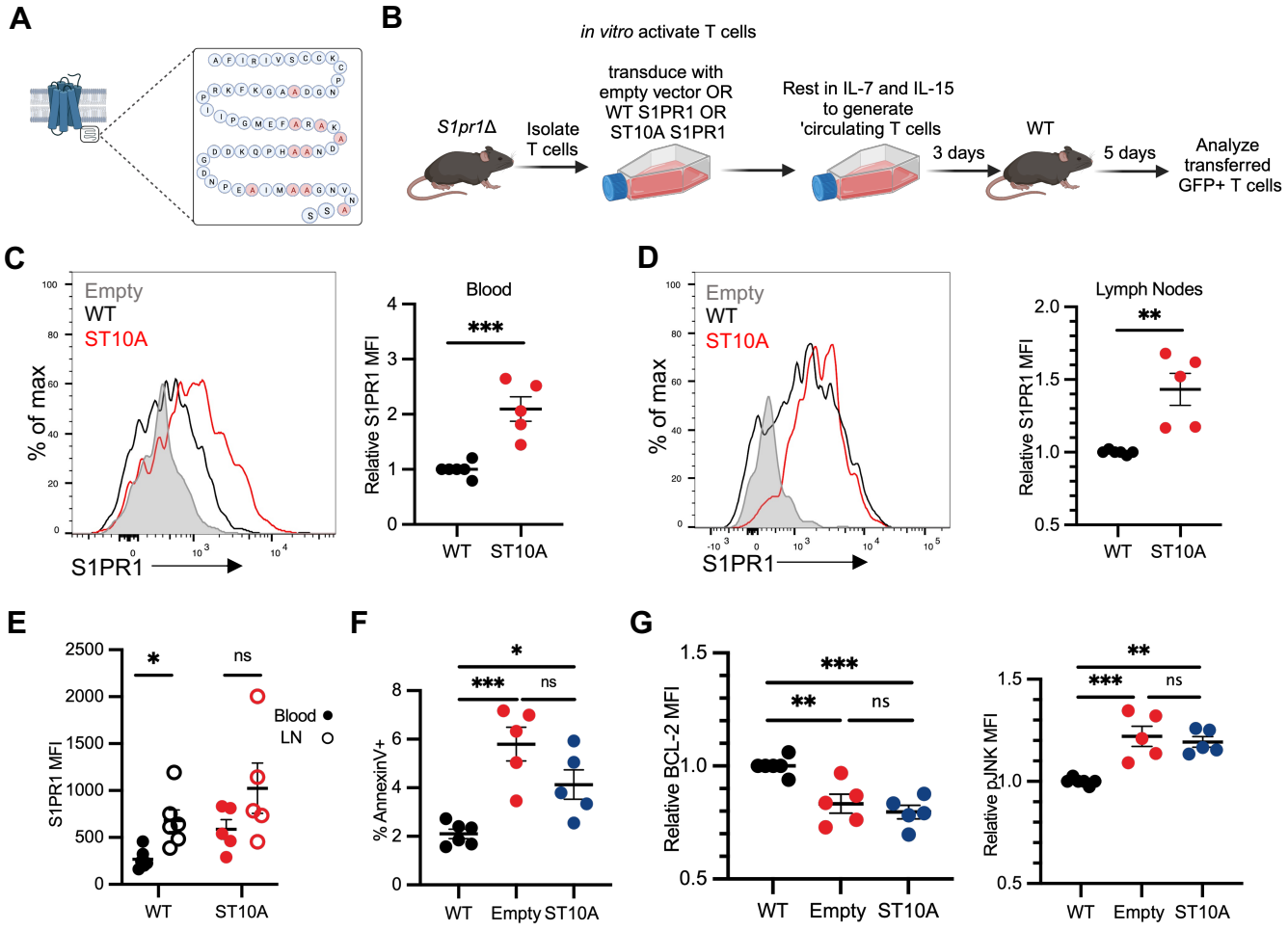
A
B
in vitro activate T cells
S1pr1Δ
Isolate T cells
transduce with empty vector OR WT S1PR1 OR ST10A S1PR1
Rest in IL-7 and IL-15 to generate 'circulating T cells
3 days
WT
5 days
Analyze transferred GFP+ T cells
C
Empty
WT
ST10A
% of max
S1PR1
Blood
Relative S1PR1 MFI
***
WT
ST10A
D
Empty
WT
ST10A
% of max
S1PR1
Lymph Nodes
Relative S1PR1 MFI
**
WT
ST10A
E
S1PR1 MFI
*
ns
Blood
LN
WT
ST10A
F
% AnnexinV+
*
***
ns
WT
Empty
ST10A
G
Relative BCL-2 MFI
***
**
ns
WT
Empty
ST10A
Relative pJNK MFI
**
***
ns
WT
Empty
ST10A

Figure 7

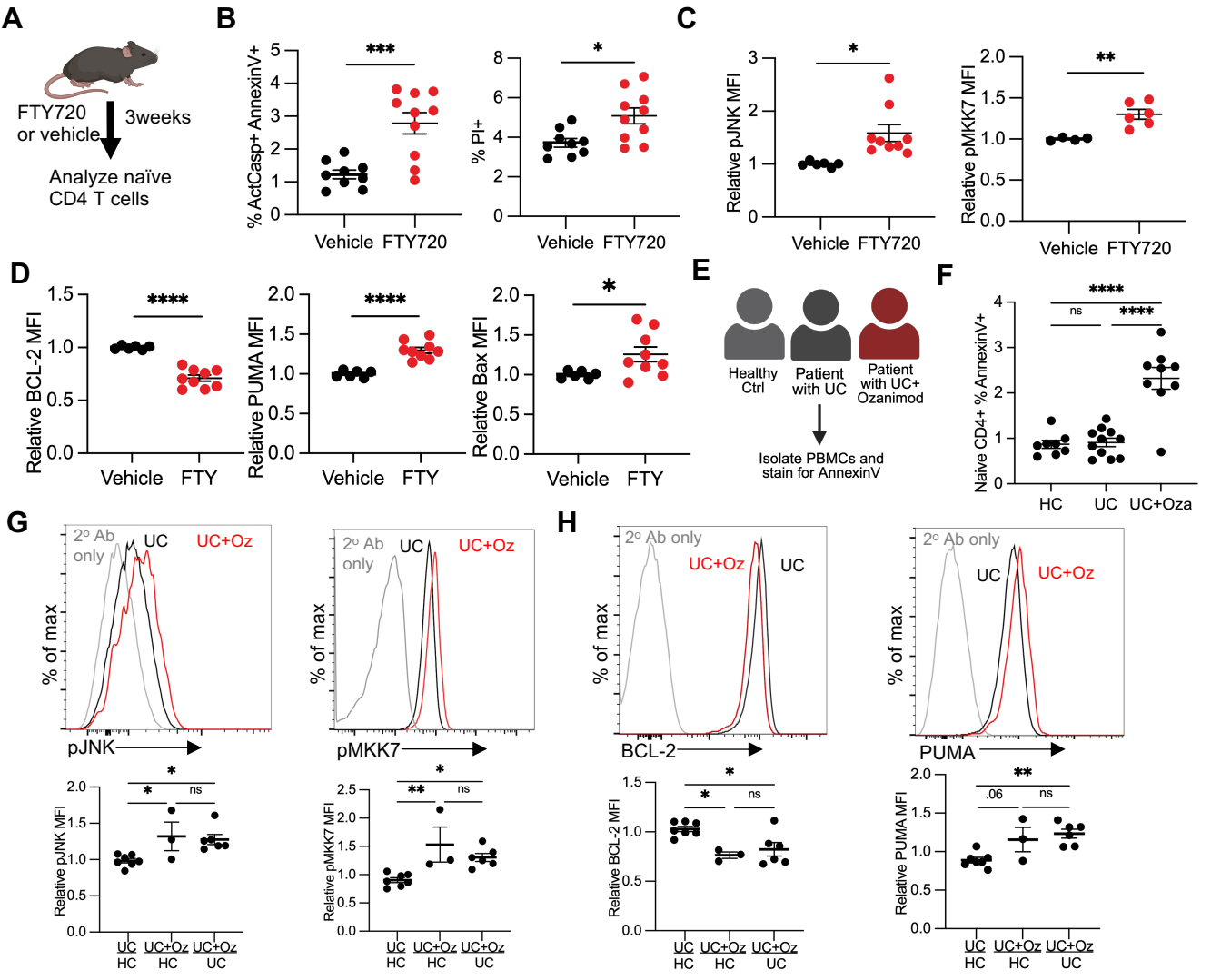
A
FTY720
or vehicle
3weeks
Analyze naïve
CD4 T cells
B
% ActCasp+ AnnexinV+
Vehicle FTY720
% PI+
Vehicle FTY720
C
Relative pJNK MFI
Vehicle FTY720
Relative pMKK7 MFI
Vehicle FTY720
D
Relative BCL-2 MFI
Vehicle FTY
Relative PUMA MFI
Vehicle FTY
Relative Bax MFI
Vehicle FTY
E
Healthy Ctrl
Patient with UC
Patient with UC+ Ozanimod
Isolate PBMCs and stain for AnnexinV
F
Naive CD4+ % AnnexinV+
HC UC UC+Oza

G
2º Ab only
UC
UC+Oz
% of max
pJNK
Relative pJNK MFI
UC HC
UC+Oz HC
UC+Oz UC
pMKK7
Relative pMKK7 MFI
H
BCL-2
Relative BCL-2 MFI
PUMA
Relative PUMA MFI

Figure 8

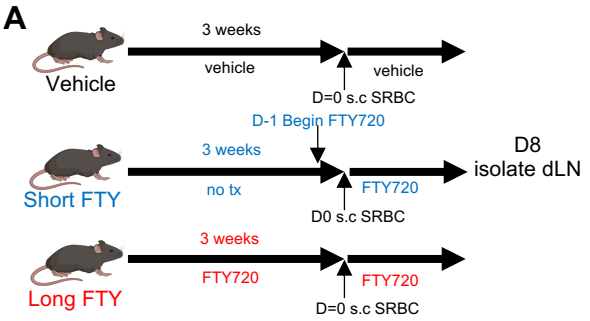
A
Vehicle
3 weeks
vehicle
vehicle
D=0 s.c SRBC
D-1 Begin FTY720
Short FTY
3 weeks
no tx
FTY720
D0 s.c SRBC
D8
isolate dLN
Long FTY
3 weeks
FTY720
FTY720
D=0 s.c SRBC

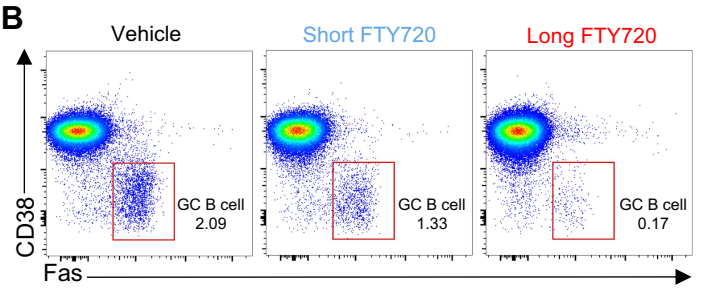
B
Vehicle
Short FTY720
Long FTY720
CD38
Fas
GC B cell
2.09
GC B cell
1.33
GC B cell
0.17

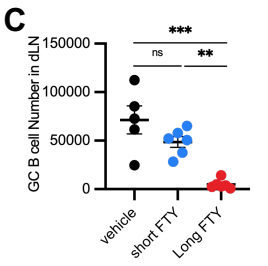
C
GC B cell Number in dLN
150000
100000
50000
0
***
ns
**
vehicle
short FTY
Long FTY

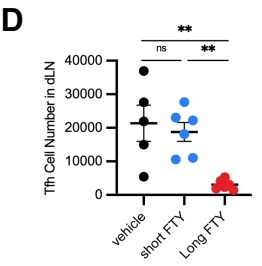
D
Tfh Cell Number in dLN
40000
30000
20000
10000
0
**
ns
**
vehicle
short FTY
Long FTY

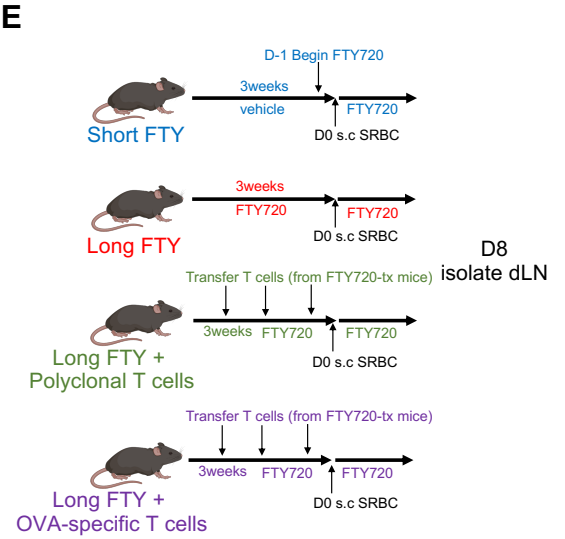
E
D-1 Begin FTY720
3weeks
vehicle
FTY720
D0 s.c SRBC
Short FTY
3weeks
FTY720
FTY720
D0 s.c SRBC
Long FTY
D8
isolate dLN
Transfer T cells (from FTY720-tx mice)
3weeks
FTY720
FTY720
D0 s.c SRBC
Long FTY +
Polyclonal T cells
Transfer T cells (from FTY720-tx mice)
3weeks
FTY720
FTY720
D0 s.c SRBC
Long FTY +
OVA-specific T cells

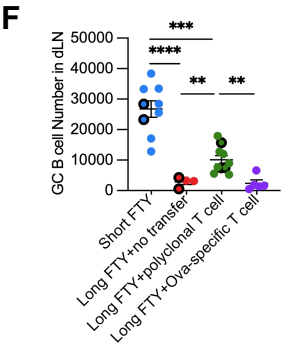
F
GC B cell Number in dLN
50000
40000
30000
20000
10000
0
***
****
**
**
Short FTY
Long FTY+no transfer
Long FTY+polyclonal T cell
Long FTY+Ova-specific T cell

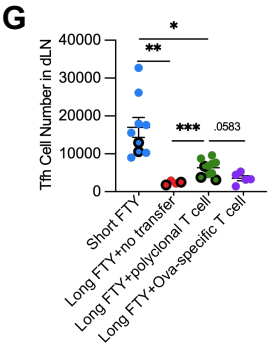
G
Tfh Cell Number in dLN
40000
30000
20000
10000
0
*
**
***
.0583
Short FTY
Long FTY+no transfer
Long FTY+polyclonal T cell
Long FTY+Ova-specific T cell

Figure 9

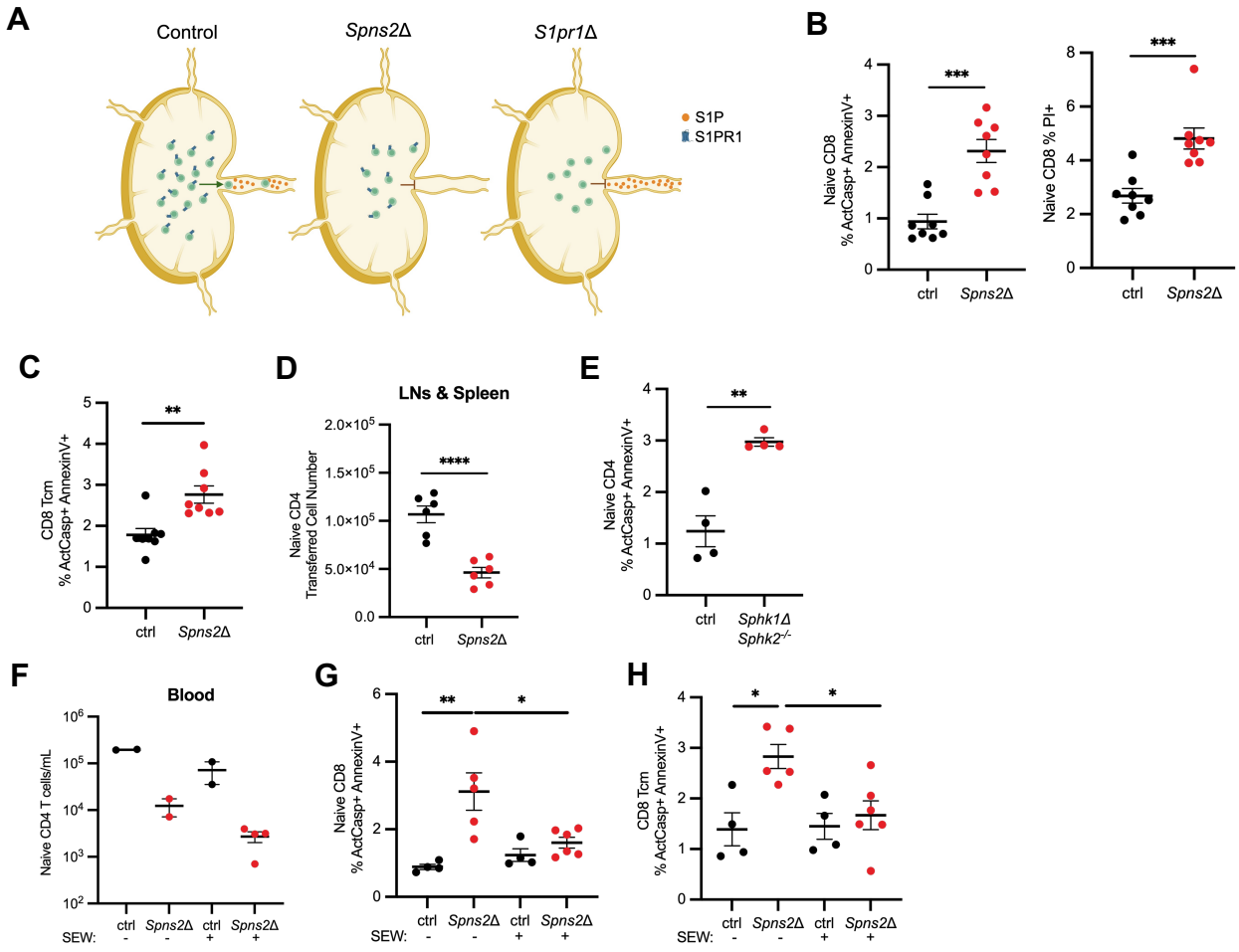

Supplementary Figure 1: SPNS2-derived S1P and S1PR1 prevent apoptotic death of naïve T cells.

A) Schematic of naïve T cell trafficking. Left: In a normal mouse, S1P is high in lymph compared to LN, and T cells express S1PR1. S1PR1 guides T cells out of the low-S1P environment of LN into the high-S1P environment of lymph. Center: In a SPNS2-deficient mouse, lymph S1P is lost. T cells still express S1PR1, but without lymph S1P to attract T cells out of the LN, T cells do not exit. Right: In an S1PR1-deficient mouse, S1P remains high in lymph compared to LN. However, without S1PR1, T cells cannot sense the S1P gradient and do not exit. Created with biorender.com.

B-C) *Spns2*$^{f/f}$ *UBC*-CreERT2 mice and littermate controls were treated with tamoxifen, and 3-4 weeks later LN T cells were analyzed by flow cytometry. (B) Frequency of ActCasp+ AnnexinV+ and PI+ cells among naïve CD8+ T cells. (C) Frequency of ActCasp+ AnnexinV+ among CD8+ Tcm (CD62L+CD44hi). Compilation of 4 experiments with n=8 mice for both groups.

D) *Spns2*$^{f/f}$ *UBC*-CreERT2 mice and littermate controls were treated with tamoxifen. 3-4 weeks after tamoxifen treatment, the mice received 1x10^6 CD45.1+ lymphocytes intravenously. Three weeks post-transfer, naïve CD4+ CD45.1+ T cells remaining in the recipient animals were enumerated (total reflects sum of cells in skin-draining LN, mesenteric LN, and spleen). Compilation of 3 experiments with n=6 mice per group.

E) Frequency of ActCasp+ AnnexinV+ cells among naïve CD4+ T cells in LN of *Sphk1*$^{f/f}$*Sphk2*$^{-/-}$ *Lyve1*-Cre mice and littermate controls. Compilation of 2 experiments with n=4 mice for both groups.

F-H) *Spns2*$^{f/f}$ *Lyve1*-Cre mice and littermate controls were treated with 10mg/kg SEW-2871 or vehicle daily. After ten days of treatment, T cells were analyzed by flow cytometry. (E) Number of naïve CD4+ T cells in the blood of *Spns2*Δ mice and littermate controls, with and without SEW-2871 treatment. Frequency of ActCasp+ AnnexinV+ cells among (G) naïve CD8+ T cells and (H) CD8+ Tcm (CD62L+CD44hi) in LN of *Spns2*Δ mice and littermate controls, with and without SEW-2871 treatment. Compilation of 3 experiments with n=3-4 mice per group.

Statistical analysis: Student's t test was performed for panels B-E. One-way ANOVA was performed for panel G-H. *p ≤ 0.05, **p ≤ 0.01, ***p ≤ 0.001, ****p ≤ 0.0001, N.S. non-significant.

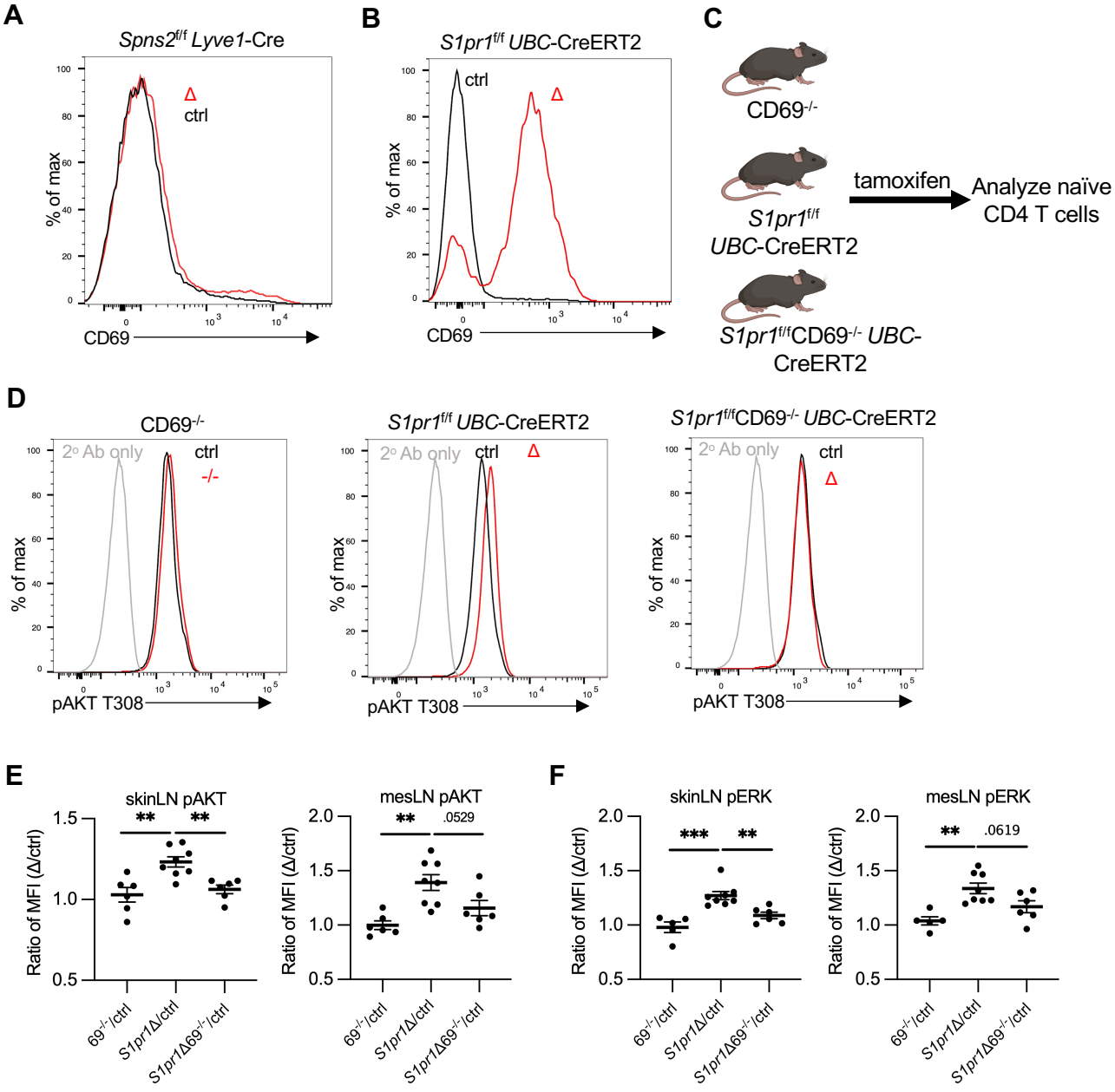

Supplementary Figure 2: CD69 regulates increased pAKT and pERK in S1PR1-deficient naïve T cells.

Text: One distinction between naïve T cells from *Spns2*Δ and *S1pr1*Δ mice is that naive *S1pr1*Δ T cells have high surface levels of the C-type lectin CD69 compared to controls, while naïve T cells from *Spns2*Δ mice do not have detectable surface CD69 (Figures S2A-S2B). CD69 and S1PR1 play antagonistic roles on the cell surface (71). Naïve T cells express high levels of S1PR1, which binds basal CD69 and maintains its low surface expression. A recently activated T cell robustly increases *Cd69* transcription, which shifts the balance; the increased CD69 binds S1PR1 and forces its internalization, keeping T cells at the site of activation. Naïve *S1pr1*Δ T cells have high levels of surface CD69 at baseline. Much remains to be learned about CD69's function, but we hypothesized that surface CD69 might promote AKT and ERK signaling, as these pathways are normally induced early during T cell activation. To test this, we crossed *S1pr1*$^{f/f}$*UBC*-CreERT2 with *Cd69*$^{-/-}$ mice(64) and asked whether loss of CD69 reduced AKT and ERK phosphorylation in *S1pr1*Δ T cells (Figure S2C). *S1pr1*Δ naïve T cells had increased expression of pAKT and pERK compared to littermate controls and *Cd69*$^{-/-}$ T cells, but *S1pr1*Δ; *Cd69*$^{-/-}$ naïve T cells had similar expression of pAKT and pERK to controls and *Cd69*$^{-/-}$ T cells (Figures S2D-S2F). This suggests that high expression of CD69 in *S1pr1*Δ naïve T cells partially explains the increased pAKT and pERK.

Legend: A-B) Representative histogram of CD69 surface expression on naïve CD4+ T cells from LN of (A) *Spns2*Δ and (B) *S1pr1*Δ (red) or littermate control (black) mice.

C-F) *S1pr1*$^{f/f}$ *UBC*-CreERT2 mice, CD69$^{-/-}$ mice, or *S1pr1*$^{f/f}$ *UBC*-CreERT2; CD69$^{-/-}$ mice and their respective littermate controls were treated with tamoxifen. 3-4 weeks later, T cells from either skin-draining LN or mesenteric LN were analyzed by flow cytometry for pAKT and pERK expression. (C) Experiment diagram. (D) Representative histograms of pAKT expression by naïve CD4 T cells from skin-draining LN of the indicated mice. (E-F) Compilation. Each point represents ratio of (E) pAKT or (F) pERK geometric MFI in naïve CD4+ T cells between a *S1pr1*Δ, CD69$^{-/-}$, or *S1pr1*Δ CD69$^{-/-}$ mouse and its respective littermate control. Compilation of 6 experiments with n=6-8 mice per group.

Statistical analysis was performed using One-way ANOVA with multiple comparisons. *p ≤ 0.05, **p ≤ 0.01, ***p ≤ 0.001, ****p ≤ 0.0001, N.S. non-significant.

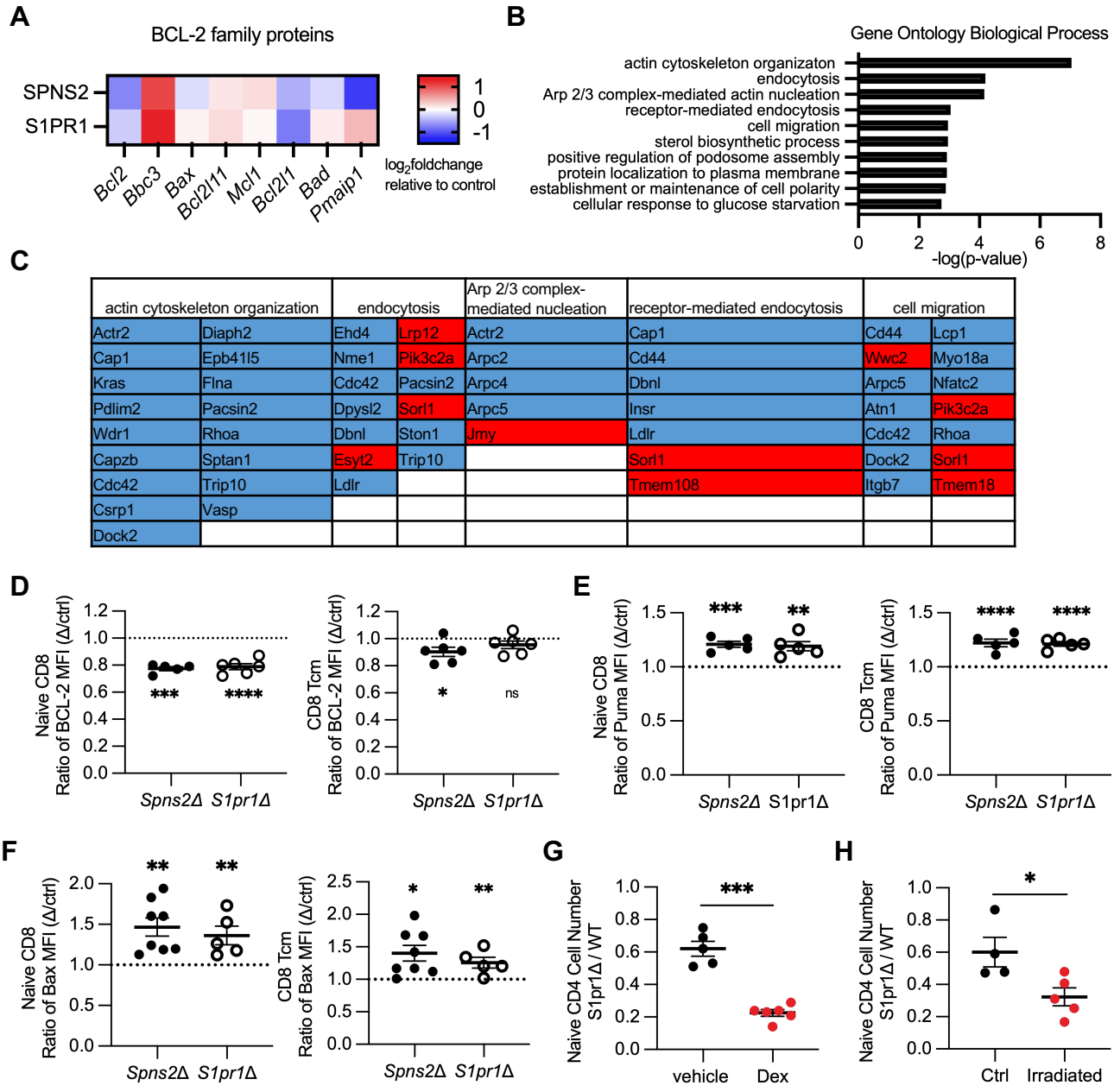

Supplementary Figure 3: Expression of BCL-2 family proteins in the absence of S1P signaling.

A-C) For SPNS2: CD45.2 *Spns2*$^{f/f}$ *Lyve1*-Cre mice or CD45.2 littermate control mice were lethally irradiated and reconstituted with WT CD45.1/.2 bone marrow. After reconstitution, naïve CD4 T cells were isolated and RNA-Seq was performed. For S1PR1: a 50:50 mixture of CD45.2 UBC-GFP: CD45.2 *S1pr1*$^{f/f}$ *UBC*-CreERT2 or CD45.2 *UBC*-GFP: CD45.2 *S1pr1*$^{f/f}$ control bone marrow was transferred into lethally irradiated CD45.1/.2 WT mice. After reconstitution, mice were treated with tamoxifen. Four weeks after tamoxifen treatment, naïve T cells were isolated and RNA-Seq was performed. (A) Heatmap of BCL-2 family proteins in naïve CD4 T cells from *Spns2*Δ and *S1pr1*Δ mice. Heatmap represents $\log_2$fold change of genes from either *Spns2*Δ mice or *S1pr1*Δ mice relative to control cells. (B) Differentially expressed genes shared between both *Spns2*Δ and *S1pr1*Δ datasets were used to generate top 10 Gene Ontology (GO) biological process using DAVID Bioinformatics Resource. (C) Differentially expressed genes shared between both *Spns2*Δ and *S1pr1*Δ datasets listed under top Gene Ontology Biological Processes. Red: up in the absence of S1P signaling. Blue: down in the absence of S1P signaling.

D-F) Expression of BCL-2 family members in naïve CD8+ T cells and CD8+ Tcm (CD62L+CD44hi) from LN of *Spns2*Δ or *S1pr1*Δ mice and littermate controls. (D) Compilation of BCL-2 expression. Each point represents the ratio of BCL-2 geometric MFI between a *Spns2*Δ or *S1pr1*Δ mouse and its littermate control. Compilation of 5-6 experiments with n=5-7 pairs per group. (E) As in (D) for PUMA. Compilation of 4-5 experiments with n=4-5 pairs per group. (F) As in (D) for BAX. Compilation of 6 experiments with n=5-8 pairs per group.

G-H) *S1pr1*Δ and littermate control lymphocytes were co-transferred (1:1 by naïve CD4 T cell counts) intravenously into WT recipients. The transferred cells were labeled with CellTrace Violet or CellTrace Yellow, and dyes were swapped between experiments. 24 hours later, recipients were treated with either 2 mg/kg dexamethasone or 1 gy irradiation. 24 hours later, dye-labeled naïve CD4 T cells in LN were enumerated. Compilation of ratio of number of naïve CD4+ T cells from *S1pr1*Δ mice vs its littermate control recovered in recipients. (G) 2 mg/kg dexamethasone treatment. Compilation of 3 experiments with n=5-7 mice per group. (H) 1 gy irradiation. Compilation of 2 experiments with n=4-5 mice per group.

Statistical analysis was performed using Student's t test. *p ≤ 0.05, **p ≤ 0.01, ***p ≤ 0.001, ****p ≤ 0.0001, N.S. non-significant.

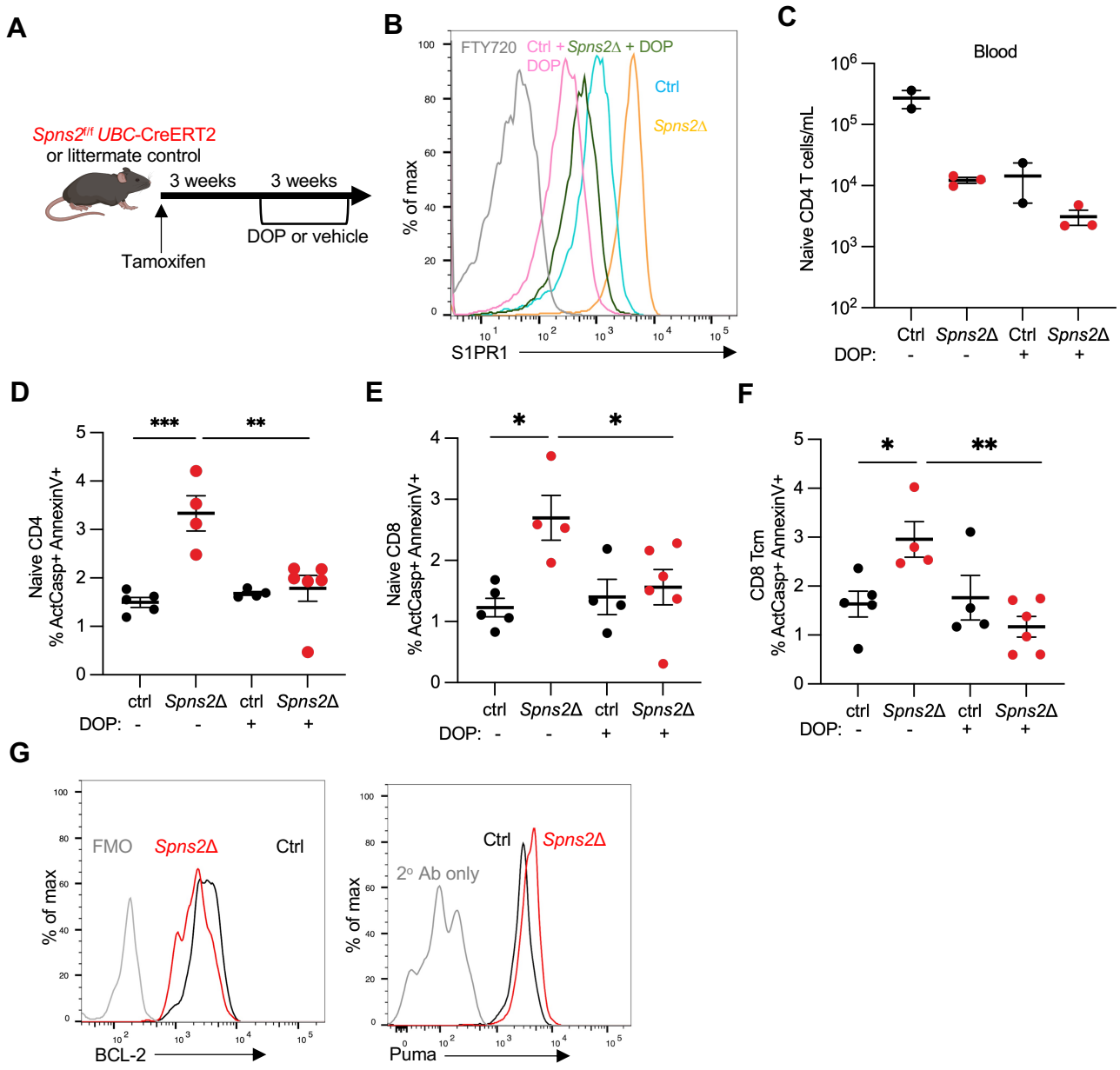

Supplementary Figure 4: BCL-2 family proteins regulate S1PR1-dependent naïve T cell survival.

A-F) *Spns2*$^{f/f}$ *UBC*-CreERT2 mice and littermate controls were treated with tamoxifen. At least 3 weeks later, mice were treated with 30mg/l DOP and 10mg/l sucrose, or sucrose alone, in the drinking water. After 3 weeks of DOP treatment, LN T cells were analyzed by flow cytometry. (A) Experiment design. (B) Representative histogram of surface S1PR1 expression on naïve CD4+ T cells from LN of *Spns2*Δ mice and littermate controls, with and without DOP treatment. (C) Number of naïve CD4+ T cells in the blood of *Spns2*Δ mice and littermate controls, with and without DOP treatment. Compilation of 2 experiments with n=2-3 per group. (D) Frequency of ActCasp+ AnnexinV+ cells among naïve CD4+ T cells in LN of *Spns2*Δ mice or littermate controls, with or without DOP treatment. Compilation of 3 experiments with n=4-6 mice per group. Frequency of ActCasp+ AnnexinV+ cells among (E) naïve CD8+ T cells and (F) CD8+ Tcm (CD62L+CD44hi) in LN of *Spns2*Δ mice or littermate controls, with and without DOP treatment. Compilation of 3 experiments with n=4-6 per group.

G) Representative histograms of BCL-2 and PUMA expression in *Bax*$^{-/-}$ naïve CD4+ T cells transferred to *Spns2*$^{f/f}$ *Lyve1*-Cre mice or littermate controls.

Statistical analysis was performed using one-way ANOVA was multiple comparisons. *p ≤ 0.05, **p ≤ 0.01, ***p ≤ 0.001, ****p ≤ 0.0001, N.S. non-significant.

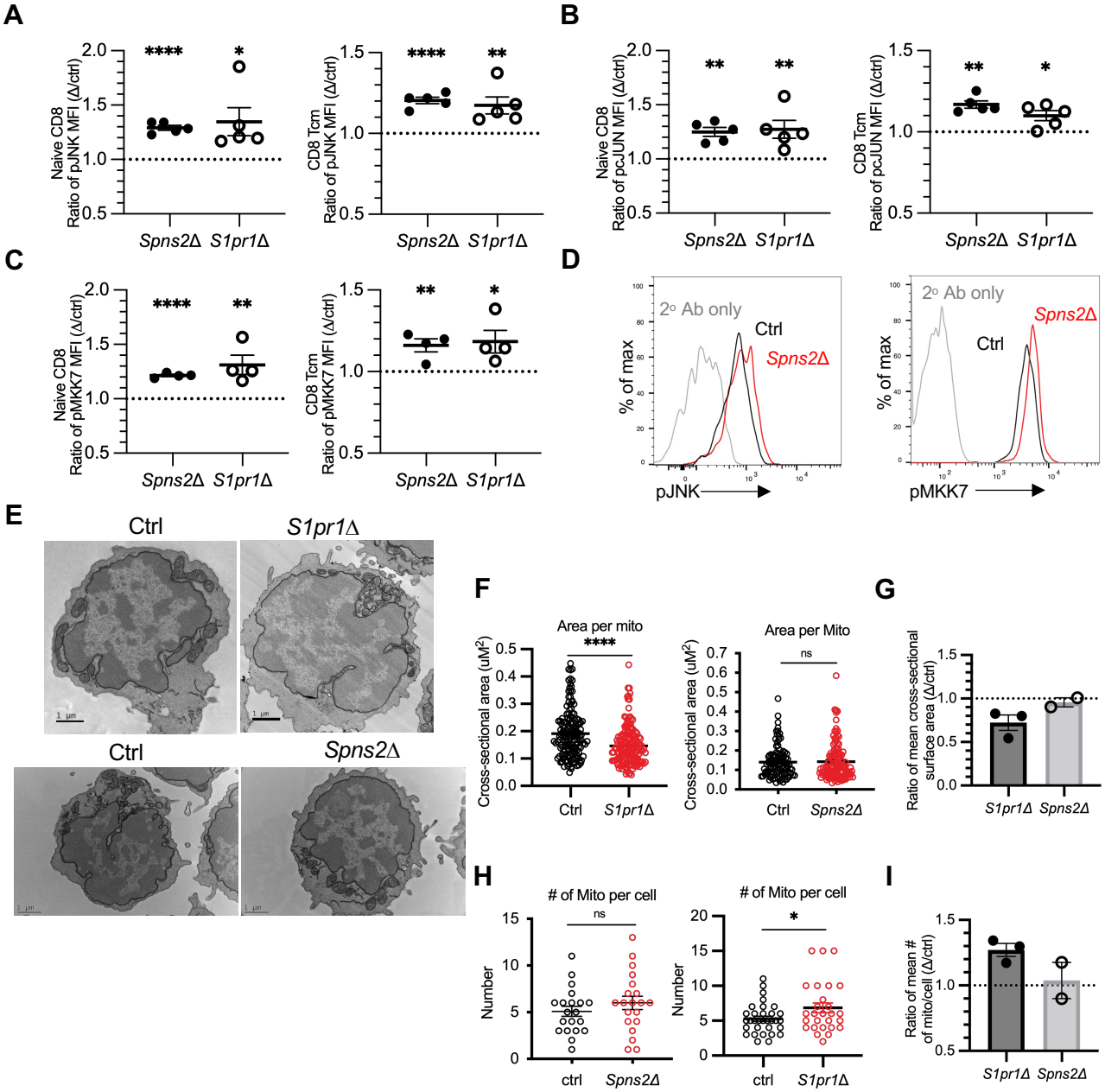

Supplementary Figure 5: JNK signaling regulates S1P-dependent naïve T cell survival.

A-C) Expression of phosphorylated JNK pathway proteins in naïve CD8+ T cells and CD8+ Tcm (CD62L+CD44hi) from LN of *Spns2*Δ or *S1pr1*Δ mice and littermate controls, analyzed by flow cytometry. (A) Compilation of relative MFI values for pJNK. Relative values represent expression in one individual mouse divided by the mean value of littermate control mice in that experiment. Compilation of 4-5 experiments with n=5 pairs per group. (B) As in (A) for pcJUN. Compilation of 4-5 experiments with n=4-5 pairs per group. (C) As in (A) for pMKK7. Compilation of 4 experiments with n=4 pairs per group.

D) Representative histograms of pJNK and pMKK7 expression in *Bax*$^{-/-}$ naïve CD4+ T cells transferred to *Spns2*$^{f/f}$ Lyve1-Cre mice or littermate controls.

E-I) Electron microscopy analysis of mitochondria in naïve CD4+ T cells sorted from LN. (E) Representative images of mitochondria within naïve CD4+ T cells from LN of a *S1pr1*Δ mouse and its littermate control or a *Spns2*Δ^{Lyve1} mouse and its littermate control. (F) Cross-sectional area of individual mitochondria, from one representative set of mice examining at least 20 cells per genotype. (G) Compilation of the ratio of the mean cross-sectional area of mitochondria in naïve CD4+ T cells of *S1pr1*Δ mice vs their littermate controls (3 pairs in 3 experiments) or of *Spns2*Δ mice vs their littermate controls (2 pairs in 2 experiments). (H) Number of mitochondria per cell, from one representative set of mice examining at least 20 cells per genotype. (I) Compilation of the ratio of the mean number of mitochondria per cell of *S1pr1*Δ mice vs their littermate controls (3 pairs in 3 experiments), or of *Spns2*Δ mice vs their littermate controls (2 pairs in 2 experiments).

Statistical analysis was performed using Student's t test. *p ≤ 0.05, **p ≤ 0.01, ***p ≤ 0.001, ****p ≤ 0.0001, N.S. non-significant.

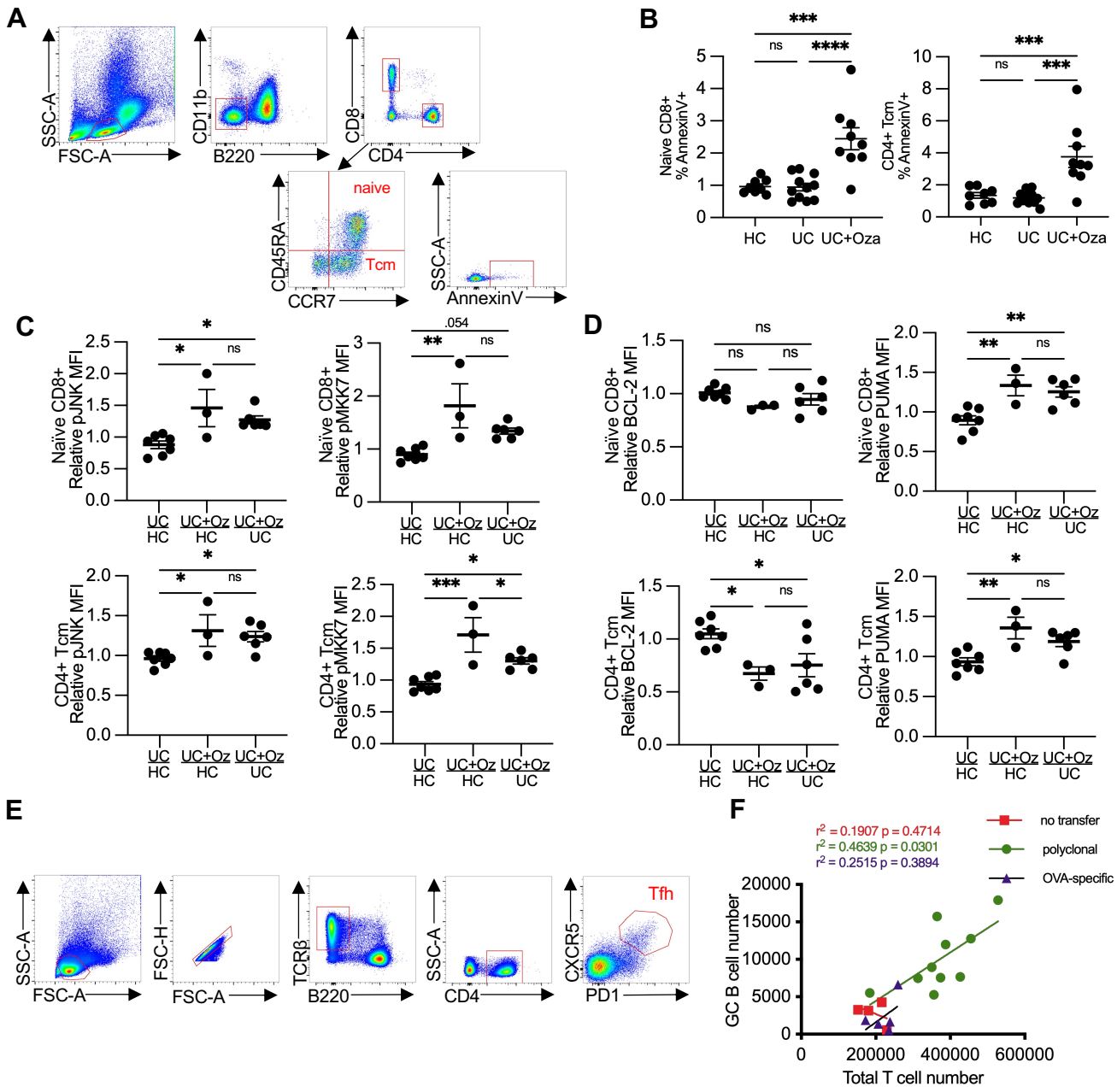

Supplementary Figure 6: S1PR1 modulators impair T cell survival in humans and germinal center responses in mice.
A-D) PBMCs were isolated from blood samples of UC patients treated with ozanimod (UC+Oza), UC patients not treated with ozanimod (UC), or healthy controls (HC), and analyzed by flow cytometry. (A) Gating strategy to analyze naïve CD4+, naïve CD8+, and CD4+ Tcm. (B) Frequency of AnnexinV+ cells among naïve CD8+ T cells or among CD4+ Tcm cells. Compilation of 10 experiments with n=8-11 per group. (C) Compilations of pJNK and pMKK7 relative geometric MFI values from naïve CD8+ T cells or from CD4+ Tcm cells, calculated as in Fig. 7F. Compilation of 10 experiments with n=3-7 per group. (D) Compilations of relative MFI values for BCL-2 and PUMA from naïve CD8+ T cells or from CD4+ Tcm cells. Compilation of 10 experiments with n=3-7 per group.
E) Gating strategy to identify Tfh cells.
F) Correlation between total T cell numbers and GC B cell numbers from 'Long FTY + no transfer' group, 'Long FTY + polyclonal T cells' group, and 'Long FTY + OVA-specific T cells' group.
Statistical analysis was performed using one-way ANOVA with multiple comparisons for panels B-D. *p ≤ 0.05, **p ≤ 0.01, ***p ≤ 0.001, ****p ≤ 0.0001, N.S. non-significant.

Supplementary Table 1: Characteristics of ulcerative colitis patients and healthy controls

	Healthy Controls (n=8)	UC+ No Ozanimod (n=11)	UC + Ozanimod (n=9)
Sex			
Female	5 (62.5%)	2 (18.2%)	4 (42.9%)
Male	3 (37.5%)	9 (81.8%)	5 (57.1%)
Race			
White	6 (75%)	6 (54.5%)	5 (55.6%)
Black	0	0	3 (33.3%)
Asian	0	2 (18.2%)	1 (11.1%)
Other/mixed	2 (25%)	3 (27.3%)	0
Hispanic ethnicity	0	1 (9.1%)	0
Age at Encounter (years; median, IQR)	32 (28)	33 (17)	29 (7.5)
Age at IBD diagnosis (years; median, IQR)	-	26 (15)	24 (7)
Duration of disease (years; median, IQR)		6 (10)	4 (4)
Maximum ulcerative colitis extent	-		
Proctitis		1 (9.1%)	2 (22.2%)
Left-sided		0	3 (33.3%)
Extensive colitis		9 (81.8%)	4 (42.9%)
Inflammatory biomarkers within 30 days	-		
C-rp (median, IQR)		0.7 (2.7)	1.3 (4.6)
Fecal calpro (median, IQR)		262 (250)	839 (435)
Mayo endoscopic subscore within 30 days	-		
0		4 (36.3%)	1
1		2 (18.2%)	0
2		2 (18.2%)	4 (42.9%)
3		1 (9.1%)	2 (22.2%)
Not assessed		2 (18.2%)	2 (22.2%)
IBD therapy exposure history	-		
Mesalamines		10 (90.9%)	9 (100%)
Corticosteroids		9 (81.8%)	8 (88.9%)
Immunomodulators		2 (18.2%)	2 (22.2%)
Anti-TNF		4 (36.3%)	2 (22.2%)
Vedolizumab		1 (9.1%)	2 (22.2%)
JAK inhibitor		0	2 (22.2%)

Supplementary Table 2: Materials used in the study

Reagent or Resource	Source	Identifier
Antibodies		
APC-conjugated Streptavidin	BioLegend	catalog no. 405207
APC-conjugated anti-mouse CD44 (IM7)	BioLegend	catalog no. 103012 RRID:AB_312963
APC-conjugated anti-human CCR7 (G043H7)	BioLegend	catalog no. 353213 RRID:AB_10915474
APC-conjugated anti-mouse CD45.2 (104)	BioLegend	catalog no. 109814 RRID: AB_389211
APC-Cy7-conjugated anti-human CD11b (MI/70)	BioLegend	catalog no. 101226 RRID: AB_830642
APC-e780-conjugated anti-mouse CD8a (5.3-6.7)	Thermo Fisher Scientific	catalog no. 47-0081-82 RRID: AB_1272185
APC-e780 conjugated anti-TCR-beta (H57-597)	Thermo Fisher Scientific	catalog no. 47-5961-82 RRID: AB_1272173
Biotinylated Affinipure Fragment Donkey anti-Rat	Jackson Immunoresearch	catalog no. 712-066-153 RRID: AB_2340649
BUV395-conjugated anti-mouse CD4 (GK1.5)	BD Biosciences	catalog no. 740208 RRID: AB_2734761
BUV395- conjugated anti- B220 (RA3-6B2)	BD Biosciences	catalog no.563793 RRID: AB_2738427
BV421-conjugated anti-mouse CD62L (MEL-14)	BioLegend	catalog no. 104436 RRID:AB_2562560
BV421-conjugated anti-human CD45RA (HI100)	BioLegend	catalog no. 304130 RRID:AB_10965547
BV510-conjugated anti-mouse CD62L (MEL-14)	BioLegend	catalog no. 104441 RRID: AB_2561537
BV650-conjugated anti-mouse CD25 (PC61)	BioLegend	catalog no. 102038 RRID: AB_2563060
FITC-conjugated anti-mouse CD45.1 (A20)	BioLegend	catalog no. 110706 RRID: AB_313495
FITC-conjugated anti-mouse CD62L (MEL-14)	BioLegend	catalog no. 104408 RRID: AB_313095
PE-conjugated anti-mouse CD69 (H1.2F3)	BioLegend	catalog no. 104508 RRID: AB_313111
PE-conjugated anti-mouse CD44 (IM7)	BioLegend	catalog no. 103024 RRID:AB_493687
PE-conjugated anti-mouse CD45.1 (A20)	BioLegend	catalog no. 110708 RRID:AB_313496

PE-conjugated anti-mouse CD127 (A7R34)	BioLegend	catalog no.135010 RRID: AB_1937251
PE-conjugated anti-human CCR7 (G043H7)	BioLegend	catalog no. 353203 RRID:AB_10916391
PE-conjugated anti-mouse BCL-2 (BCL/10C4)	BioLegend	catalog no. 633508 RRID: AB_2290367
PE-conjugated anti-human BCL-2 (100)	BioLegend	catalog no. 658707 RRID:AB_2563282
PerCP-Cy5.5-conjugated anti-mouse B220 (RA3-6B2)	BioLegend	catalog no. 103236 RRID: AB_893354
PerCP-Cy5.5-conjugated anti-mouse CD44 (IM7)	BioLegend	catalog no. 103032 RRID: AB_2076204
PerCP-Cy5.5-conjugated anti-mouse CD45.2 (104)	BioLegend	catalog no. 109828 RRID:AB_893350
Rat anti-mouse S1PR1 (713412)	R&D Systems	catalog no. MAB7089
Rabbit anti-phospho AKT T308 (D25E6)	Cell Signaling Technology	catalog no. 13038S
Rabbit anti-phospho-p44/p42 ERK1/2 Thr 202/Tyr 204	Cell Signaling Technology	catalog no. 9101L
Rabbit anti-phospho-S6 Ribosomal protein (Ser235/236)	Cell Signaling Technology	catalog no. 2211L
Rabbit polyclonal anti-PUMA	ProSci	catalog no. 3043
Mouse anti-Bax (6A7)	Thermo Fisher Scientific	catalog no. MA5-14003 RRID: AB_10979735
Rabbit anti-phospho-JNK1/2 (D12H7L17)	Thermo Fisher Scientific	catalog no. 700031 RRID: AB_2532273
Mouse anti-phospho-cJUN (KM-1)	Santa Cruz Biotechnology	catalog no. sc-822
Rabbit anti-phospho-MKK7 (Ser271,Thr 275) (MKK7S271T275-R4F9)	Thermo Fisher Scientific	catalog no. MA5-28042
Rabbit anti-phospho-CREB (87G3)	Cell Signaling Technology	catalog no. 9198S
Alexa Fluor 647-conjugated donkey anti-rabbit IgG	Jackson Immunoresearch	catalog no. 711-605-152 RRID:AB_2492288
Alexa Fluor 647-conjugated donkey anti-mouse IgG	Jackson Immunoresearch	catalog no. 715-605-150 RRID: AB_2340862
Alexa Flour 647-conjugated anti-mouse BCL-2 (BCL/10C4)	BioLegend	catalog no. 633510 RRID:AB_2274702
Biotinylated anti-mouse CD8a (5.3-6.7)	BioLegend	catalog no. 100704 RRID: AB_312743
Biotinylated anti-mouse CD11c (N418)	BioLegend	catalog no. 117304 RRID: AB_313773

Biotinylated anti-mouse CD11b (M1/70)	BioLegend	catalog no. 101204 RRID: AB_312787
Biotinylated anti-mouse NK1.1 (PK136)	BioLegend	catalog no. 108704 RRID: AB_313391
Biotinylated anti-mouse Ter119 (TER-119)	BioLegend	catalog no. 116204 RRID:AB_313705
Biotinylated anti-mouse CD19 (6D5)	BioLegend	catalog no. 115504 RRID:AB_313639
Biotinylated anti-mouse B220 (RA3-6B2)	BioLegend	catalog no. 103204 RRID:AB_312989
Biotinylated anti-mouse CD25 (PC61)	BioLegend	catalog no. 102004 RRID:AB_312853
Biotinylated anti-mouse TCR γ/δ (GL3)	BioLegend	catalog no. 118103 RRID:AB_313827
Biotinylated anti-mouse CD44 (IM7)	BioLegend	catalog no. 103003 RRID:AB_312954
InVivoMab anti-mouse CD3ε (145-2C11)	Bio X Cell	catalog no. BE0001-1 RRID:AB_1107634
InVivoMab anti-mouse CD28 (37.51)	Bio X Cell	catalog no. BE0015-1 RRID:AB_1107628
InVivoMab rat IgG2A isotype control (2A3)	Bio X Cell	catalog no. BE0089 RRID:AB_1107769
InVivoMab anti-mouse CD127 (A7R34)	Bio X Cell	catalog no. BE0065 RRID:AB_1107590
Chemicals, Peptides, and Recombinant Proteins		
PBS	Gibco	catalog no. 14190250
RPMI-1640	Gibco	catalog no. 11875119
DMEM	Corning	catalog no. 10014CV
OptiMEM	Gibco	catalog no. 51985034
Tamoxifen	Sigma-Aldrich	catalog no. T5648
ABT-199	Tocris	catalog no. 6960
SP600125	Selleckchem	catalog no. S1460
H-89	Selleckchem	catalog no. S1582
JNK-IN-8	MedChemExpress	catalog no. HY-13319
Dexamethasone	Sigma-Aldrich	catalog no. D1756
SEW-2871	Cayman Chemical	catalog no. 10006440
Fingolimod	Cayman Chemical	catalog no. 10006292
4-deoxypyridoxine-HCl	Sigma-Aldrich	catalog no. D0501
Lipofectamine 2000	Thermo Fisher	catalog no. 11668027
Polybrene	Sigma-Aldrich	catalog no. TR-1003
Lymphoprep	Stem Cell Technologies	catalog no. 7801
Recombinant murine IL-7	Peprotech	catalog no. 217-17

Recombinant human IL-2	Peprotech	catalog no. 200-02
Recombinant murine IL-15	Peprotech	catalog no. 210-15
Fas ligand	Enzo Life Sciences	catalog no. ALX-850-014-KI02
TRIzol LS	Thermo Fisher Scientific	catalog no. 10296010
Linear Acrylamide	Thermo Fisher Scientific	catalog no. am9520
Magnisort Negative Selection Beads	Thermo Fisher Scientific	catalog no. MSNB-6002-71
FITC-conjugated caspACE-VAD-FMK	Promega	catalog no. G7461
Pacific Blue-conjugated AnnexinV	BioLegend	catalog no. 640918
APC-conjugated AnnexinV	BioLegend	catalog no. 640920
AnnexinV Binding Buffer	BioLegend	catalog no. 422201
Corn Oil	Sigma-Aldrich	catalog no. C8267
Sucrose	Sigma-Aldrich	catalog no. S9378
Tween 20	Sigma-Aldrich	catalog no. P1379
Tween 80	Sigma-Aldrich	catalog no. P1754
PEG400	Sigma-Aldrich	catalog no. PX1286B-2
Critical Commercial Assays		
Rneasy Plus Micro Kits	QIAGEN	catalog no. 74034
Rnase-free Dnase set	QIAGEN	catalog no. 79254
eBioscience FoxP3 staining kit	Thermo Fisher Scientific	catalog no. 00-5523-00
Cytofix/Cytoperm Kit	BD Biosciences	catalog no. 554714
CellTrace Yellow Cell Proliferation Kit for Flow Cytometry	Thermo Fisher Scientific	catalog no. C34567
CellTrace Violet Cell Proliferation Kit for Flow Cytometry	Thermo Fisher Scientific	catalog no. C34557
Live/DEAD Fixable Blue Dead Cell Stain Kit	Thermo Fisher Scientific	catalog no. L23105
Experimental Models: Cells/ Cell Lines		
Grk2$^{f/-}$*Cd4*-Cre and Grk2$^{f/+}$ Cd4-Cre bone marrow	Laboratory of Jason Cyster	Arnon et al., 2011
Platinum-E (plat-E) cell line	Laboratory of T Kitamura	Morita et al., 2000
Sheep Red Blood Cells	Colorado Serum Company	catalog no. 31112
Experimental Models: Organisms/ Strains		
C57BL/6J	Jackson Laboratory	RRID: IMSR_JAX:000664
B6.SJL-*Ptprc*^{a}*Pepc*^{b}/BoyJ	Jackson Laboratory	RRID: IMSR_JAX:002014
Spns2$^{f/f}$	This laboratory	Mendoza et al., 2012
S1pr1$^{f/f}$	Jackson laboratory	RRID: IMSR_JAX:019141
UBC-CreERT2	Jackson laboratory	RRID: IMSR_JAX:007001
Lyve1-Cre	Laboratory of Jason Cyster	Pham et al., 2010
Bax$^{-/-}$	Jackson Laboratory	RRID: IMSR_JAX:002994

MHCII$^{-/-}$	Jackson Laboratory	RRID: IMSR_JAX:003584
Cd69$^{-/-}$	Laboratory of Jason Cyster	Murata et al., 2003
Sphk1$^{f/f}$	Laboratory of Jason Cyster	Pappu et al., 2007
Sphk2$^{-/-}$	Jackson Laboratory	RRID: IMSR_JAX:019140
OT-I: C57BL/6-Tg(TcraTcrb)1100Mjb/J	Jackson Laboratory	IMSR_JAX:003831
OT-II: B6.Cg-Tg(TcraTcrb)425Cbn/J	Jackson Laboratory	IMSR_JAX:004194
Recombinant DNA		
pMIGR1	Addgene (gift from Warren Pear)	RRID: Addgene_27490
WT S1PR1-pMIGR1	This laboratory	
ST10A S1PR1-pMIGR1	This laboratory	
Software and algorithms		
GraphPad Prism 9.0	GraphPad	https://www.graphpad.com/scientific-software/prism/
FlowJo v 10	TreeStar	https://www.flowjo.com/solutions/flowjo
FACSDiva v8.02	BD Biosciences	https://www.bdbiosciences.com/en-us/instruments/research-instruments/research-software/flow-cytometry-acquisition/facsdiva-software
Biorender	Biorender	www.biorender.com
ImageJ v 1.49	NIH	https://imagej-nih-gov.ezproxy.med.nyu.edu/ij/
Other		
LSRII Flow Cytometer	BD Biosciences	N/A
Beckman Coulter Multisizer 3	Beckman Coulter	catalog no. 383601
LightCycler 480 System	Roche Diagnostics	catalog no. 5015243001